# 1 Involvement of Arabidopsis Acyl Carrier Protein 1 in PAMP-triggered immunity



- Funding: This project was supported by the Hatch Project from USDA-NIFA-OHO01392; the
- Ohio Agricultural Research and Development Center (OARDC) seed grant OHOA1591; startup
- 20 fund from OARDC and Ohio State University to YX.

#### Abstract:

21

22

23

24

25

26

27

28

29

30

31

32

33

34

35

36

37

Plant fatty acids (FAs) and lipids are essential in storing energy and act as structural components for cell membranes and signaling molecules for plant growth and stress responses. Acyl Carrier Proteins (ACPs) are small acidic proteins that covalently bind the fatty acyl intermediates during the elongation of FAs. The Arabidopsis thaliana ACP family has eight members. Through reverse genetic, molecular, and biochemical approaches, we have discovered that ACP1 localizes to the chloroplast and limits the magnitude of pattern-triggered immunity (PTI) against the bacterial pathogen Pseudomonas syringae pathovar tomato (Pto). The mutant acp1 plants have reduced levels of linolenic acid (18:3), which is the primary precursor for the biosynthesis of the phytohormone jasmonic acid (JA), and a corresponding decrease in the abundance of JA. Consistent with the known antagonistic relationship between JA and salicylic acid (SA), acp1 mutant plants also accumulate higher level of SA and display the corresponding shifts in JA- and SA-regulated transcriptional outputs. Moreover, the methyl JA and linolenic acid treatments cause an apparently enhanced decrease of resistance against *Pto* in *acp1* mutants than that in wild-type plants. The ability of ACP1 to prevent this hormone imbalance likely underlies its negative impact on PTI in plant defense. Thus, ACP1 links FA metabolism to stress hormone homeostasis to be negatively involved in PTI in Arabidopsis plant defense.

38

39

**Keywords:** acyl carrier protein, fatty acids, plant immunity, PTI, plant hormones

40

41

42

45

46

47

48

49

50

51

52

53

54

55

56

57

58

59

60

61

62

63

64

#### 43 **INTRODUCTION:**

Pseudomonas syringae pathovar tomato (Pto) is an agriculturally important pathogen that causes the bacterial speck disease on tomato plants resulting in yield and economic losses (Bashan, 1997; Bashan and de-Bashan, 2002). Pto strain DC3000 (Pto DC3000) is also pathogenic to the model plant Arabidopsis thaliana, which provides a classic system to study the pathogenesis mechanisms and dynamics of plant-pathogen interactions (Xin et al., 2018). In addition to Pto, more than 50 different P. syringae pathovars can infect more than 200 plant species and cause destructive diseases, from leaf speck to stem cankers (Buttimer et al., 2017). Plants defend themselves against P. syringae and the other pathogenic microbes through multi-layered innate immunity (Jones and Dangl, 2006). Basal defense constitutes a first layer that often protects plants entirely or limits the extent of pathogen growth. Critical to basal defense is the pattern triggered immunity (PTI), which is activated upon the interaction of microbe-associated molecular patterns (MAMPs) with transmembrane pattern recognition receptors (PRRs), such as between a 22 amino acid epitope of the flagellin protein (flg22) and the kinase receptor FLAGELLIN SENSITIVE2 (FLS2) (Jones and Dangl, 2006). Pathogens secrete virulence effectors, such as secreted proteins and toxins, limiting the basal defense and thus facilitating infection. The second layer of plant defense, effector triggered immunity (ETI), is elicited when a resistance (R) protein directly or indirectly recognizes a corresponding effector (Takemoto and Jones, 2005; Jones and Dangl, 2006; Jones et al., 2016). Emerging experimental evidence indicates the significant mutual influences and the overlapping downstream defense outputs between PTI and ETI, suggesting the intricate and integrative interactions between these two layers of plant immunity (Ngou et al., 2021; Yuan et al., 2021b; Yuan et al., 2021a).

Plant defense responses include reactive oxygen species (ROS) production, cell wall fortification, shifts in hormone levels and gene expression patterns, *etc.* (Spoel and Dong, 2012). ROS is produced rapidly upon the MAMP engagement of a PRR (Liu et al., 2009). In addition to providing antimicrobial activity, ROS are signaling molecules that influence plant defense (Dat et al., 2000; Mittler et al., 2004; Kwak et al., 2006). For example, the exogenous H<sub>2</sub>O<sub>2</sub> enhances the accumulation of SA, which further upregulates ROS production (Shirasu et al., 1997). Cell wall fortification, which includes the deposition of the polysaccharide callose, is a somewhat later output of defense activation (Luna et al., 2011). Plant hormones play critical roles in plant defense as well. For example, SA-signaling activates both local and systemic defense responses against *Pto* (Gao et al., 2015). Conversely, JA-signaling increases the susceptibility of Arabidopsis to *Pto* (Zheng et al., 2012). These observations are consistent with numerous studies demonstrating the antagonism between SA- and JA-signaling (Xin and He, 2013). The interplay between fatty acid and lipid biosynthetic pathways with these defense hormones is a significant knowledge gap for understanding the plant immune responses.

Fatty acids (FAs) and lipids are critical for many biological processes of plants. Their involvement in energy storage is critical for plant growth and development. They are also important structural components of plant membranes (Brown et al., 2009). FAs and lipids have been implicated as signaling molecules contributing to systemic acquired resistance (SAR). For instance, glycerol-3-phosphate, a phosphoric ester of glycerol and a critical component of glycerophospholipids, is a mobile inducer of the broad-spectrum and long-lasting plant disease resistance characteristic of SAR (Chanda et al., 2011; Lim et al., 2020). FAs and lipids also play diverse functions in plant defense (Zoeller et al., 2012; Gao et al., 2014; Gao et al., 2015). SSI2 encodes a stearoyl-acyl carrier protein desaturase, which mediates the conversion of stearic acid

89

90

91

92

93

94

95

96

97

98

99

100

101

102

103

104

105

106

107

108

109

110

(18:0) to oleic acid (18:1) to regulate the levels of unsaturated fatty acids in Arabidopsis plants. The reduced levels of oleic acid (18:1 FA) in Arabidopsis plants with a mutation of *SSI2* correlate with the increased ROS, SA, callose deposition levels, spontaneous cell death, and enhanced resistance against *Pto* (Kachroo et al., 2001). A mutation in Acyl Carrier Protein 4 (ACP4) restored the levels of 18:1 FA in *ssi2* plants, which in turn suppresses all the *ssi2*-triggered physiological and defense phenotypes. The ability of ACP4 to affect SSI2 related function was due to its effect on the glycerol-3-phosphate (G3P) acyltransferase (ACT1)-catalyzed reaction (Xia et al., 2009).

Acyl Carrier Proteins (ACPs) are central components for fatty acid biosynthesis. In plants, de novo FA biosynthesis is carried out by the conserved reactions starting with acetyl-CoA in the chloroplast (Byers and Gong, 2007). The synthesis process is performed via multiple elongation cycles (Marrakchi et al., 2002). The ACPs are small (~9kD) acidic polypeptides that covalently bind the fatty acyl intermediates through a phosphopantetheine linker during the elongation process (Chan and Vogel, 2010). The fatty acyl chain is extended by acetyl-CoA, two carbon units per cycle, until C16 or C18 acyl-ACPs are formed and exported for the long-chain FAs and lipid biosynthesis. Several ACP isoforms have been characterized in multiple plant species, including spinach (Ohlrogge et al., 1979), soybean (Ohlrogge and Kuo, 1985), barley (Hansen and von Wettstein-Knowles, 1991), cotton (Song and Allen, 1997), rapeseed (SAFFORD et al., 1988), olive (Cultrera et al., 2014) and Arabidopsis (Hloušek-Radojčić et al., 1992). Although the critical roles of ACPs in FA biosynthesis have been demonstrated, the roles of various ACP isoforms in plants remain unclear (Bonaventure and Ohlrogge, 2002). Of the eight genes encoding ACPs in the genome of the model plant Arabidopsis, five were predicted to be localized to the plastid [ACP1 (At3g05020), ACP2 (At1g54580), ACP3 (At1g54630), ACP4 (At4g25050), ACP5 (At5g27200)] and three to the mitochondria [mtACP1 (At2g44620), mtACP2 (At1g65290), and

mtACP3 (At5g47630)] through the use of antibodies and mass spectrometry (Meyer et al., 2007; Meier et al., 2010). The transcript and protein levels of ACPs in plants are influenced by diverse biotic and abiotic stresses (Ruuska et al., 2002). For instance, phosphate starvation increases the protein abundance of plastidal ACP isoforms (ACP1/2/3/4) in roots (Lan et al., 2012). ACP4 contributes to SAR dependent on its critical role for the cuticle formation in Arabidopsis leaves (Xia et al., 2009; Lim et al., 2020). It was reported that ACP5 could contribute to the plant resistance against salt stress, possibly through an influence of FAs on the Na<sup>+</sup>/K<sup>+</sup> ratio. Indeed, overexpression of *ACP5* increased the levels of palmitic acid (16:0) and decreased the levels of oleic acid (18:1) (Huang et al., 2017). The functions of the other ACP isoforms in fatty acid biosynthesis and biotic or abiotic stresses are poorly understood.

In this study, we demonstrate that ACP1 limits the magnitude of PTI by influencing fatty acid biosynthesis. Specifically, the reduced levels of linolenic acid (18:3 FA) in the leaves of *acp1* mutant plants underlie the enhanced resistance against *Pto* DC3000 through the effects on the JA and SA accumulation and the related signaling pathways.

#### **RESULTS**

# Identification and characterization of acp1 mutant plants.

ACP is an essential cofactor during the synthesis of fatty acids in bacteria and plants. The phosphopantetheine binding domain (PP-binding superfamily), conserved in ACP proteins, is the prosthetic group of ACP, which acts as a linker for the attachment of the activated fatty acid and amino-acid groups via a phosphodiester bond (Roujeinikova et al., 2002; Crawford et al., 2008; Meier et al., 2010). All eight Arabidopsis ACP isoforms share this conserved domain (**Figure 1a**). To further investigate the relationships of the ACPs, the protein sequences of all 8 ACP isoforms

134

135

136

137

138

139

140

141

142

143

144

145

146

147

148

149

150

151

152

153

154

155

were uploaded to Clustal Omega for phylogenetic analysis by multiple sequence alignments. The protein sequence of ACP2 is 90% similar to ACP3. Furthermore, ACP1 is more closely related to ACP5 than the other ACP isoforms (**Figure 1b**).

Here, the roles of ACPs against biotic stress, especially in response to the bacterial pathogen Pto DC3000 were studied. The altered gene expression of ACPs in infected plant leaves might indicate their contribution to plant defense responses. The abundance of ACP transcripts was measured in the wild type (WT) Col-0 leaves before and 6 hours after the Pto DC3000 inoculation, which revealed that the expression of multiple ACPs changed in response to the pathogen infection. The basal expression of different isoforms was variable in WT Col-0 leaves. ACP4 was expressed the highest in Arabidopsis leaves. The *Pto* infection reduced the transcript levels of *ACP1*, *ACP4*, and ACP5 but increased ACP3, mtACP2, and mtACP3 (Figure S1). The T-DNA insertion lines of all the 8 Arabidopsis ACP genes were obtained from ABRC (Arabidopsis Biological Resource Center at The Ohio State University), and the homozygous lines were identified using the protocol designed the Salk Institute Genomic by Analysis Laboratory (http://signal.salk.edu/tdnaprimers.2.html). The resistance levels of all the eight *acp* mutant plants were investigated against the Pto DC3000 infection. It was found that acp1 mutant plants showed the enhanced resistance against *Pto* DC3000 compared to WT plants (unpublished data). Based on the enhanced resistance to *Pto*, the role of ACP1 in plant immunity was further investigated. For acp1 mutant lines, the insertion sites of the two T-DNA insertion lines (acp1-1 and acp1-2) are within the promoter and first intron, respectively (**Figure S2**). The transcript levels of *ACP1* were compared between the two acpl homozygous mutants and WT Col-0 plants by quantitative realtime PCR (qPCR). The ACP1 transcript levels were significantly lower in the mutant lines than WT (Figure 1c).

FAs are critical constituents of cellular membranes, which maintain cellular structure and function. FAs are also essentially involved in the precursor formations of suberin, cell wall, cutin, and wax, which are pivotal for constructing the structural barriers and vital for plant growth and development (Beisson et al., 2007; Maejima et al., 2014). In our study, the visual examination revealed no effects of either *acp1* mutant allele on plant growth or development. Physiological parameters, such as biomass, plant height, and chlorophyll content, did not differ between the *acp1* mutants and WT plants (**Figure S3&S4**). Therefore, the defective function of *ACP1* does not appear to impair the growth and development of Arabidopsis plants significantly.

# Subcellular localization of ACP1 in the transiently transformed Nicotiana benthamiana.

ACP1 is annotated as a plastidial ACP (Hloušek-Radojčić et al., 1992; Meyer et al., 2007; Meier et al., 2010). And it was predicted to be localized in chloroplast, which contains a chloroplast transit peptide with 30 amino acids as an N-terminal sorting signal based on the analysis results using the software of TargetP (https://services.healthtech.dtu.dk/service.php?TargetP-2.0) and iPSORT (https://ipsort.hgc.jp/how.html). To confirm the subcellular prediction, we constructed a GFP (green fluorescent protein)-tagged version of full-length ACP1 (ACP1-GFP) to determine the subcellular localization of ACP1 *in planta*. The empty vector pyBA1122-35S-GFP was applied as a negative control. ACP1-GFP and empty vector-GFP were co-expressed in *N. benthamiana* leave with PT-mCherry, a plastid organelle marker, respectively (Nelson et al., 2007). The fluorescence signals were checked three days after the infiltration through the confocal laser scanning microscopy. The green fluorescence signal of ACP1-GFP was found to overlap with the red fluorescence signal of PT-mCherry (Figure 2a). Meanwhile, the green signal of the empty vector-GFP was diffusely distributed (Figure 2b). Thus, it indicated that ACP1 localizes to the chloroplast in Arabidopsis plants.

#### Responses of acp1 plants to the Pto infection.

To confirm the defense phenotype of acp1 mutant plants, two acp1 mutants and WT plants were syringe infiltrated with a suspension of  $5\times10^5$  CFU (colony forming unit)/ml of Pto DC3000. WT Col-0 plants showed more severe chlorotic and necrotic disease symptoms than acp1 mutant plants three days after the inoculation (**Figure 3a**). Meanwhile, the bacterial growth was measured at 0- and 3-days post-inoculation. The Pto DC3000 proliferated significantly less in the acp1 mutants than WT at 3 days post-inoculation (**Figure 3b**). To further investigate the role of ACP1 in PTI, the expression levels of three PTI marker genes, including FRK1, At1g51890, and At2g17740 (Cheng et al., 2013; Guo et al., 2014), were monitored upon Pto DC3000 infection. Notably, the induction of all the three PTI marker genes was significantly enhanced in acp1 mutants at 6 and 48 hours post-inoculation, compared with WT plants (**Figure 3c**). These results indicate that ACP1 is negatively involved in Arabidopsis resistance against the Pto DC3000 infection.

### The acp1 mutant plants showed reduced levels of C18:3 fatty acid.

As ACPs are the critical factors for FA synthesis, the abundance of total FAs was measured from the 4-week-old *acp1* mutants and WT plant leaves following the established procedures (Xia et al., 2009). Of the C16 and C18 FAs measured, only C18:3 FA differed significantly in the *acp1* mutants compared to WT plants (**Figure 4a**). The reduced accumulation of C18:3 FA in the mutant plants indicates a requirement of ACP1 for the biosynthesis of this class of FA in Arabidopsis leaves. To further investigate the level change of C18:3 FA in WT and *acp1* mutant plants against the pathogen infection, the abundance of C18:3 FAs from *acp1* mutants and WT plant leaves were measured 48 hours after the *Pto* DC3000 and buffer MgCl<sub>2</sub> inoculation, respectively. We observed that *acp1* mutant plants accumulated significantly lower levels of C18:3 FA than WT plants with

buffer MgCl<sub>2</sub> treatment, which is similar to the condition without any treatment (**Figure 4b**). And the difference of C18:3 FA abundance between *acp1* mutants and WT plants was more apparent in response to the pathogen infection (**Figure 4b**). These data suggest that ACP1 displays a significant role in C18:3 FA accumulation in response to the *Pto* pathogen infection. Since linolenic acid (18:3 FA) is the primary precursor for the biosynthesis of plant hormone jasmonic acid (JA) (Mueller et al., 1993; Santino et al., 2013), thus *acp1* alleles may have a lower JA accumulation/response, and this may affect the outcome of the interaction with *Pto* with increased resistance level against the *Pto* DC3000 in *acp1* mutants.

# Reduced levels of JA in acp1 mutant plants disrupt the balance of JA- and SA-signaling.

Synthesis of JA, its methyl ester (MeJA), and its active isoleucine conjugates (JA-Ile/Leu) mostly begin with the C18:3 FA in the chloroplast (Ruan et al., 2019; Wasternack and Strnad, 2019). The reduced levels of C18:3 FA led us to hypothesize that the *acp1* mutants: 1) would have the reduced level of JA biosynthesis, and 2) as a result of antagonism, the SA level would be consequently increased. To test these hypotheses, the free JA, JA-Ile/Leu (JA-isoleucine/leucine), free SA, and SAG (SA-glycoside) levels in the *acp1* mutants and WT plants were quantified before and after the *Pto* pathogen inoculation. The related hormones and hormone-conjugate levels did not differ between the *acp1* mutants and WT plants before the *Pto* DC3000 treatment. However, the *acp1* mutants accumulated significantly lower JA and JA-Ile/Leu (**Figure 5a&5b**) and higher levels of SA and SAG following the challenges with the *Pto* DC3000 (**Figure 5c&5d**).

The altered levels of SA and JA are likely associated with the differential transcriptional outputs. To further characterize the influence of *ACP1* on JA- and SA-signaling, the transcriptional levels of several genes in JA- and SA-related pathways were analyzed and compared between *acp1* mutants and WT plants by qPCR. Firstly, the expression of the SA biosynthesis gene (*SID2*) and

226

227

228

229

230

231

232

233

234

235

236

237

238

239

240

241

242

243

244

245

246

247

SA response gene (PRI) were analyzed. Although the SA and SAG accumulation did not show significant differences between acp1 mutants and WT plants without the Pto DC3000 inoculation, acp1 mutants had significantly higher SID2 and PR1 transcriptional levels than WT plants. Consistent with the hormone results, significantly higher transcriptional levels of SID2 and PR1 were present in acp1 mutants, relative to WT plants, at 6- and 48-hours post-inoculation with the Pto DC3000 (Figure 6a&6b). Next, the expression levels of the JA receptor gene (COII) and a JA response gene (PDF1.2) were analyzed between the acp1 mutants and WT plants. Again, despite the lack of difference in JA levels in unchallenged acpl mutants, it was found that the transcript levels of PDF1.2 were significantly lower in acp1 mutants, relative to WT, before the pathogen challenge. At 6- and 48-hours post-inoculation with Pto DC3000, the acp1 mutants showed decreased *PDF1*.2 and *COI1* gene expression than WT (**Figure 6c&6d**). The transcription factor MYC2 has been well studied as a critical component in the crosstalk of SA and JA, which generally positively regulates JA signaling but suppresses the SA signaling against the bacterial pathogen Pto DC3000 (Cui et al., 2018; Yang et al., 2019; Gautam et al., 2021). It was reported that the myc2 mutant displayed the enhanced resistance against Pto DC3000 with the increased SA level and upregulated PR1 expression (Laurie-Berry et al., 2006). In our study, the basal transcript level of MYC2 was decreased in acp1 mutants than in WT plants before Pto DC3000 treatment. And the reduced gene expression of MYC2 maintained in acp1 mutants after Pto DC3000 infection (Figure 6e). We also found that the basal transcript levels of several other JA synthesis-related genes were significantly decreased in acp1 mutants than in WT plants (Figure S5). Altogether, the hormone levels and expression of hormone pathway-related genes are consistent with the interpretation that acp1 mutants may enhance the resistance against Pto DC3000 by repressing the JA-signaling pathway and upregulating the SA-signaling pathway.

### Methyl JA and linolenic acid treatments decreased the resistance against Pto in acp1 mutants.

248

249

250

251

252

253

254

255

256

257

258

259

260

261

262

263

264

265

266

267

268

269

270

The acp1 mutants with the enhanced resistance against Pto showed a significantly reduced level of C18:3 FA in response to the *Pto* DC3000 infection, accompanied by the decrease in JA and JA-Ile/Leu accumulation as well as gene expressions associated with the JA pathway. To further investigate the role of ACP1 in the accumulation of C18:3 FA and JA against Pto, exogenous MeJA (methyl JA, 50 µM) and linolenic acid (C18:3 FA, 0.1 mM) were sprayed onto WT and acp1 mutants leaves 24 hours before the pathogen Pto DC3000 inoculation (Mata-Pérez et al., 2015; Zhao et al., 2020). The bacterial population was monitored three days after the inoculation. As expected, the MeJA treatment increased the susceptibility of WT plants to Pto DC3000 (Figure 7a) (Zhao et al., 2020). Also, MeJA treatment increased the plant susceptibility to Pto in acp1 mutants. Eventually, the acp1 mutants showed similar bacterial Pto multiplication as in WT plants with the MeJA treatment (Figure 7a). We also observed that the linolenic acid treatment increased the susceptibility of WT and mutant plants to the *Pto* infection (**Figure 7b**). Notably, although acpl showed less bacterial multiplication than WT, the magnitude of the enhanced susceptibility of acp1 mutant plants, relative to WT plants, was increased following the linolenic acid application (**Figure 7b**). Consistent with the previous results of the changes of FAs and hormone levels against the pathogen infection, these results further indicated the role of ACP1 in the accumulation of C18:3 FA and JA in the defense response to the *Pto* infection. The negative impact of ACP1 on PTI possibly links FA metabolism to the stress hormone homeostasis in plant defense.

# Enhanced PTI responses in acp1 mutant plants.

Because SA-signaling contributes positively to PTI, we speculated that the heightened PTI might be observed in *acp1* mutant plants. An early PTI response elicited by the exposure to

MAMPs is a burst of ROS. To further examine the role of ACP1 in PTI, the real-time quantification of H<sub>2</sub>O<sub>2</sub> from *acp1* mutants and WT plants exposed to flg22 was measured. The H<sub>2</sub>O<sub>2</sub> burst detected in *acp1* mutants was of greater magnitude compared to WT plants (**Figure 8a**). The H<sub>2</sub>O<sub>2</sub> accumulation was also monitored after the *Pto* DC3000 inoculation by staining the plant leaves with 3,3-diaminobenzidine tetrahydrochloride (DAB), which is oxidized by H<sub>2</sub>O<sub>2</sub> to generate a dark brown precipitate (Liu et al., 2014). The *acp1* mutants and WT plants were sprayed with a suspension of *Pto* DC3000 or buffer and then stained with DAB 24 hours later. As observed by following the flg22 treatment, the *acp1* mutants also accumulated more H<sub>2</sub>O<sub>2</sub> than WT plants following the treatment with *Pto* DC3000 (**Figure 8b&8c**), indicating *acp1* mutants could generate much more H<sub>2</sub>O<sub>2</sub> than WT plants in response to the *Pto* DC3000 inoculation.

Another commonly examined readout of PTI is the deposition of callose into defensive cell wall reinforcements (Kim et al., 2005). The callose deposition was compared between *acp1* mutants and WT plants 16 hours after the infiltration with buffer, flg22, *Pto* DC3000, or a T3SS-deficient mutant of *Pto* DC3000 (*Pto* DC3000 *hrcC*-). The callose deposition levels were similar between *acp1* mutants and WT plants with the buffer treatment. However, consistent with the enhanced SA-signaling, more callose deposition was observed in the *acp1* mutants relative to WT plants, following the infiltration with flg22, *Pto* DC3000, and *Pto* DC3000 *hrcC*- (**Figure 9a&9b**). The enhanced production of H2O2 and the deposition of callose may collectively contribute to the enhanced resistance of the *acp1* mutants against *Pto* DC3000.

#### **DISCUSSION**

ACP1 is required for Arabidopsis fatty acid biosynthesis without affecting plant growth and development.

Members of gene families often carry out discrete functions that can be challenging to tease apart. Our research reveals that ACP1, one of 8 Arabidopsis ACP isoforms, is involved in plant resistance to biotic stress. As mentioned above, ACPs are essential cofactors for fatty acid biosynthesis. Different ACP isoforms are likely required for the specific FA biosynthetic pathways (Xia et al., 2009; Huang et al., 2017). It was previously reported that overexpression of *ACP1* in Arabidopsis leaf tissues led to an increase in C18:3 FA and a decrease in C16:3 FA (Branen et al., 2001). For this study, our data indicate that a mutation in *ACP1* resulted in the significantly decreased levels of C18:3 FA in Arabidopsis plant leaves but did not affect the levels of the other FAs. And the lower level of C18:3 FA was even more apparent in *acp1* mutants than in WT plants in response to *Pto* DC3000 infection (**Figure 4a&4b**). Therefore, the data indicate that *ACP1* specifically affects C18:3 FA accumulation in Arabidopsis leaves, which may play a critical role in plant defense.

ACP1 was considered expressed at different plant tissues based on the Arabidopsis eFP Browser platform (http://bar.utoronto.ca/eplant/). It was predicted that ACP1 was expressed in leaf, root, and seed tissues of Arabidopsis plants based on the published gene profiles (Figure S6). Of all the Arabidopsis ACP isoforms, ACP4 has been reported to be abundant in Arabidopsis leaf and play a significant role in leaf FA synthesis, with the reduced levels of C16:0, C16:1, C16:3, and C18:3 FAs in the mutants. Accordingly, the acp4 mutant plants exhibited severe impaired growth and development, including the pale and undersized rosette leaves (Xia et al., 2009). In our study, the two acp1 mutants are knock-down mutant lines with the significantly decreased gene expression of ACP1 (Figure 1c). The mutants have the reduced levels of C18:3 FA (Figure 4). However, the effects of the ACP1 mutation on plant growth and development were not apparent. For instance, the plant weight, height, and chlorophyll content of the mutants were similar to WT

317

318

319

320

321

322

323

324

325

326

327

328

329

330

331

332

333

334

335

336

337

338

plants (**Figure S3&S4**). Consequently, the reduced levels of C18:3 FA hypothetically contributed to the other phenotypes of the *acp1* mutants. All these results led ACP1 to be a promising candidate for studying its roles in plant responses to biotic and possibly additional stresses.

# ACP1 influences plant immunity by controlling the defense hormone levels through FA accumulation.

Roles of FAs and lipids are emerging in plant immunity. For instance, the mutation of Acyl CoA Binding Protein 3 (ACBP3) of Arabidopsis, a member of the ACBP family which may regulate the intracellular transport of FAs and lipids, impaired the normal development of the leaf cuticle and affected both the basal and R gene-mediated defense against multiple pathogens (Xia et al., 2012). FAs and lipids and their associated factors also function as the plant systemic acquired resistance (SAR) signaling molecules. For example, azelaic acid (AzA), derived from the hydrolysis of unsaturated C18 FAs, is a mobile activator of SAR in Arabidopsis plants, at least in part by inducing the expression of genes involved in the biosynthesis of SAR inducer glycerol-3phosphate (Jung et al., 2009; Yu et al., 2013; Wang et al., 2014). Furthermore, the oxidized fatty acids, such as oxylipins, directly inhibit the mycelial growth and spore germination of diverse fungal pathogens and stimulate the plant defense gene expression in response to the Pto infection (Prost et al., 2005; Montillet et al., 2013). Plant sphingolipids are bioactive lipids that play roles in defense against abiotic and biotic stresses (Li et al., 2021). Ceramides are key intermediates in sphingolipids metabolism. Ceramides could be phosphorylated by the ceramide kinase ACD5 or catabolized by alkaline ceramidase (ACER) (Bi et al., 2014; Wu et al., 2015; Li et al., 2021). A recent study found that the JA pathway was only activated in ceramide kinase mutant acd5 mutant at the later growth stage with increased JA pathway gene expression and enhanced JA and JA-Ile/Leu accumulation. MeJA treatment enhanced the ceramide accumulation and cell death in acd5

mutant. However, the resistance to JA-related biotic stress, such as insect herbivory attack and necrotrophic pathogen *B.cinerea*, was not detected in the *acd5* mutant (Huang et al., 2021). Another report stated that double mutant *acer acd5* showed the enhanced SA pathway, oxidative stress pathway, and ceramide accumulation in response to flg22 treatment, which indicates ceramide plays a positive role in plant basal defense (Li et al., 2021). Therefore, FAs and lipids display diverse roles in plant immunity differently.

339

340

341

342

343

344

345

346

347

348

349

350

351

352

353

354

355

356

357

358

359

360

361

Here, we discover that acp1 mutants display the enhanced resistance against Pto DC3000. The plastid localized ACP1 either directly or indirectly regulates the accumulation of C18:3 FA. Notably, C18:3 FA is the primary precursor for the biosynthesis of phytohormone JA (Melotto et al., 2006; Jiang et al., 2013; Geng et al., 2014; Gimenez-Ibanez et al., 2014; Yang et al., 2019). SA is well studied to promote the effective plant resistance responses against biotrophic and hemibiotrophic pathogens such as *Pseudomonous syringae*, including the full manifestation of PTI, ETI, and further development of SAR (Vlot et al., 2009; Pieterse et al., 2012; Kim et al., 2014; Ding and Ding, 2020). The importance of JA is, at least in part, related to its antagonistic crosstalk with SA in regulating the balance between plant growth and defense responses against diverse pathogens (Xin and He, 2013; Li et al., 2019; Yang et al., 2019; Liu and Timko, 2021). Numerous studies have reported the mechanisms underlying the SA-JA antagonism, most of which are focused on SA inhibiting JA (Gupta et al., 2020). Fewer cases deciphered the decrease or loss of JA could enhance SA accumulation (Zheng et al., 2012; Liu and Timko, 2021). In our study, the acp1 mutant plants accumulated lower levels of C18:3 FA in response to the Pto pathogen infection (Figure 4b). Correspondingly, lower levels of free JA and JA-Ile/Leu and higher levels of free SA and SAG were accumulated in the mutants upon the pathogen infection, consistent with the altered transcriptional levels of JA- and SA-synthetic and responsive genes (Figure 5&6). The

enhanced susceptibility in *acp1* mutants was more apparent than in WT plants after the exogenous treatments of C18:3 and MeJA (**Figure 7**). Taken together, all these results indicate that the lower levels of C18:3 FA in *acp1* mutant plants may underlie a shift in the balance of JA- and SA-abundance and related signaling in response to the *Pto* DC3000 infection. Although the interplay between these defense hormones during the plant immune responses has been well documented, how they are linked to FAs and lipids biosynthesis is not well understood. Our findings highlight a critical role of ACP1 in influencing C18:3 FA accumulation specifically, which is associated with the plant defense hormone JA accumulation and its antagonistic interactions with SA.

# The altered SA and JA levels enhanced the PTI-related responses against the *Pto* infection in *acp1* mutant plants.

Plants can induce diverse immune responses rapidly against microbial infections to protect themselves from severe damage or death. ROS is also one of the earliest plant defense responses, which plays an essential role in plant immunity (Hirt, 2016). Reinforcement of the plant cell wall, including callose deposition, is a later and hallmark defense response elicited during PTI (Malinovsky et al., 2014). The defense hormones such as SA and JA are vital for innate immunity and connect to the other biotic stress defense pathways. The changes in the amounts and compositions of SA and JA promote plant defense responses (Yang et al., 2019; Gupta et al., 2020). Generally, SA positively affects FLS2-mediated responses, such as callose deposition and ROS burst. JA negatively regulates FLS2-mediated responses (Yi et al., 2014). *ACPI* limits the extent of both ROS production and deposition of callose (Figure 8&9). The role of defense hormones regulated by *ACPI* in these outputs of PTI points to a likely underlying mechanism. The upregulated SA-related pathway might contribute to these defense responses within the host immune system.

### The broader perspectives of ACP1 for plant defense.

The ACP1 homologs are distributed across plant species (**Table S1**), such as spinach, tomato, olive, cotton, and various brassicaceous plants. The potential role of ACP1 in plant defense across this broad range of plant species, coupled with its lack of effects on plant growth and development, points to a possible means for breeding or engineering disease-resistant plant varieties for numerous economically significant crops. In the future, gene editing approaches to modify the expression levels and function of *ACP1* in diverse crops may enhance their disease resistance against bacteria and potentially the other classes of pathogens. The detailed mechanisms of ACP1 in PTI need further investigations. For instance, the investigation of the interconnected networks of ACP1 in plant immunity as well as the related crosstalk pathways in different pathogen systems and plant species will strengthen our understanding of the functions of ACP1 and possibly the other ACP isoforms in plant immunity and facilitate their applications in enhancing plant health and yield. Furthermore, the ability of ACP1 to keep the hormone homeostasis between SA and JA indicates that ACP1 might also play critical roles in the other biotic and abiotic stresses, which deserve further investigation in the future.

#### **EXPERIMENTAL PROCEDURES**

# Plant growth and homozygous line verification.

The seeds of the mutant lines and WT Col-0 were ordered from the Arabidopsis Biological Resource Center at Columbus, USA (http://www.arabidopsis.org/). The Arabidopsis T-DNA insertion mutant lines of *ACP1* (At3g05020) were used in this study: Salk\_075428 (*acp1-1*) and CS827601(*acp1-2*). The Arabidopsis plants were grown in the growth room with 60% humidity at 22 °C under 10 hours of light and 14 hours darkness photoperiod (Fan et al., 2018). The same

408

409

410

411

412

413

414

415

416

417

418

419

420

421

422

423

424

425

426

427

428

growth condition was used for the pathogen inoculation experiments. The T-DNA insertion of the *acp* homozygous lines was identified following the instructions from Salk Institute Genomic Analysis Laboratory (http://signal.salk.edu/tdnaprimers.2.html). The primers used for genotyping and transcript confirmation are listed in **Table S2**. The *Nicotiana benthamiana* plants were grown in the same conditions as described above.

#### **Sequence Analysis.**

The protein sequences of all eight ACP isoforms were obtained from NCBI Gene-Bank (http://www.ncbi.nlm.nih.gov), which were uploaded to Clustal Omega via EMBL-EBI platform (https://www.ebi.ac.uk) for multiple protein sequence alignments. Simple Phylogeny via EMBL-EBI was used for the phylogenetic tree construction. The tree shown with straight branches and cladogram was based on the alignment with default parameters. The subcellular localization and predicted chloroplast signal peptide using **TargetP** and **iPSORT** was (https://services.healthtech.dtu.dk/service.php?TargetP-2.0;https://ipsort.hgc.jp/how.html) (Wang et al., 2021).

#### Gene expression analysis.

The total RNA for the quantitative RT-qPCR analysis was extracted from the leaf tissues. Total RNA was extracted by using Trizol (Sigma-Aldrich). The first-strand cDNA was synthesized using the Reverse Transcriptase (catalog number: 4368814, Applied Biosystem, Waltham, MA, USA). The RT-qPCR was performed using the 96-well blocks (Bio-Rad) with the CFX96 real-time PCR detection system (Bio-Rad, USA). The *ACTIN* or *UBIQUITIN* gene was used as the reference gene (Huang et al., 2017). The gene-specific primers were listed in Supplemental **Table S2**.

# **Chlorophyll content measurement.**

The plant leaves at the 4-week-old growth stage were immersed in 80% ethanol (around 30 ml) in the glass tubes wrapped in the foil at room temperature. The supernatant (1 ml) was taken from the tube every 30 mins (up to 150 mins) and finally terminated 48 hours after the treatment. The absorbance of the supernatant at 664 and 647 nm was measured by using the spectrometer (Thermo scientific Genesys 10S VIS, USA). The total micromoles chlorophyll was calculated based on the equation developed previously. The total leaf chlorophyll per gram of fresh leaf samples equals to 7.93(A664) +19.53(A647) (Lolle et al., 1997).

# Pathogen inoculation and bacterial growth quantification.

The *Pto* DC3000 and 4-week-old plants were used for the plant pathogen infection. The *Pto* DC3000 was cultured overnight on the plates with King's B medium (adding rifampin as the selective antibiotic). The bacterial cells were obtained from the plates and diluted in 10 mM MgCl<sub>2</sub>. The suspension at the concentration of 5×10<sup>5</sup> CFU (colony forming unit)/ml was syringe infiltrated into the *Arabidopsis* leaves. The residues were removed from the leaves using clean facial tissue. And then, the plants were returned to the growth room 0.5-1-hour post-inoculation. The bacterial growth was quantified three days after the inoculation as previously described (Kachroo et al., 2003; Zhao et al., 2020). For each technical replicate, three-leaf discs were collected and ground to homogeneity with a serial dilution in 10 mM MgCl<sub>2</sub>. The serial dilutions were further plated onto the King's B plate with rifampin antibiotic. The number of colonies on the plate was recorded to calculate the CFU per cm<sup>2</sup>. The log-transformed means from five technical replicates were calculated. Three independent biological repeats were applied for analysis.

#### **Exogenous Methyl JA and linolenic acid treatments**

The Methyl JA (MeJA) (Sigma-Aldrich Lot#MKBZ8786V) and linolenic acid (Acros Organics Lot#A0430295) were dissolved in ethanol and prepared as 10 mM and 3 M stock solutions, respectively. The plant leaves were evenly sprayed with mock control treatment (1% ethanol), 50 µM MeJA, and 0.1 mM linolenic acid using the vacuum-aided spray nozzle (vacuum pressure of 25 psi ) (Mata-Pérez et al., 2015; Zhao et al., 2020; Huang et al., 2021). The plants were put back in the growth room when the leaves were dry.

#### **Subcellular localization of ACP1.**

To locate ACP1 in plant cells, the full-length coding sequence of *ACP1* was amplified from the cDNA of WT plants using specific primers (**Table S2**). The pYBA1122 vector with Kanamycin selection maker includes the CaMV 35S promoter and eGFP sequence. The *ACP1* amplified fragment and the pYBA1122 vector were digested with *EcoR1* and *Sal1* enzymes. The *ACP1* fragment was ligated and inserted into the pYBA1122 vector as the ACP1-GFP. The binary plasmid of the mCherry-labeled plastid marker (PT-mCherry) was ordered from ABRC (ABRC stock name: CD3-999 with kanamycin selection). The vectors (empty vector pYBA, GFP-ACP1, and PT-mCherry) were transformed into the *A. tumefaciens* GV3101 by the electroporation method (Rossi et al., 1993). The *N. benthamiana* leaves were infiltrated with *A. tumefaciens* GV3101 harboring the PT-mCherry with ACP1-GFP or empty vector pYBA, respectively, by following the protocol described previously (Fan *et al.*, 2018). After three days of incubation, the fluorescence signals were detected under a confocal laser scanning microscopy (Nikon Eclipse 80i epifluorescent microscope, Japan).

### Fatty acid level analysis.

FA analysis was done by placing 500 ug fresh leaf tissues of 4-week-old Arabidopsis plants in the glass vials. Methylated H<sub>2</sub>SO<sub>4</sub> (2 ml), which contains 3% H<sub>2</sub>SO<sub>4</sub> in methanol and 0.001% BTH was added to the glass vials. The C17:0 FA (SIGMA Lot#SLBR3733V) was added as the internal standard. The leaf tissues were immersed in the solution. The glass vials were incubated in a water bath at 80 °C for about 30 mins. The samples were cooled down for 5-10 mins. The n-Hexane (1 ml) with 0.001% BTH was added to each glass vial. The vials were vortexed briefly and stood still for 5-10 mins. The top transparent Hexane layer was removed into the GC vials and set for GC analysis as described before (Kachroo et al., 2003). Six biological replicates were applied for each genotype.

#### The determination of hormone levels.

The plant hormone extraction and detection methods were done as described previously (Forcat et al., 2008; Peng et al., 2020; Zhao et al., 2020). Arabidopsis plant leaves were infiltrated with buffer (10mM MgCl<sub>2</sub>) or *Pto* DC3000 solution (at the concentration of 5×10<sup>5</sup> CFU/ml). The leaf samples (110 mg fresh leaf weight per sample) were collected at 0 and 48 hours post-inoculation. Each leaf sample was extracted with a 400 μl extraction buffer which contained 10% methanol and 1% acetic acid. Meanwhile, the isotope-labeled internal standards were added, including d<sub>4</sub>-SA (15 ng <sup>2</sup>H4-SA, part #D-1156, CDN Isotopes, Pointe-Claire, QC, Canada) and d<sub>5</sub>-JA (150 ng <sup>2</sup>H5-JA, part #D-6936, CDN Isotopes, Pointe-Claire, QC, Canada). The tubes with extraction buffer and internal standards were incubated on ice for 30 minutes and centrifuged for 10 minutes at 4 °C (13000 g). The supernatant was collected into new tubes. Moreover, the pellets were re-extracted with the same amount of extraction buffer without the internal standard. After two times of extraction, the pooled supernatant was further analyzed by UPLC/ESI/MS through

the Thermal Fisher Ultimate 3000 system (Thermal Fisher, Waltham, MA, USA). The C18 (3 $\mu$ m, 100 mm × 2.0 mm) column (Waters company, Milford, MA, USA) was used for UPLC separation. The mobile phase with a continuum gradient from (94.9% H<sub>2</sub>O: 5% CH<sub>3</sub>CN: 0.1% CHOOH) to (5% H<sub>2</sub>O: 94.9% CH<sub>3</sub>CN: 0.1% CHOOH) was set for around 20 mins. Multiple Reaction Monitoring (MRM) of ion pairs in negative ion mode was applied to analyze the compound. The retention time and mass transitions for SA and JA were determined using authentic standards. The transition settings for SA and JA were  $^2$ H<sub>4</sub>-SA 141.0 (97.0), SA 137.0 (93.1), SAG 299.0 (93.1),  $^2$ H<sub>5</sub>-JA 214.0 (61.0), JA 209.0 (59.1), and JA-Ile/Leu 322.0 (130.0). The daughter masses were denoted in the brackets listed above. Five technical replicates were applied for each treatment.

#### **Determination of the callose deposition.**

Callose deposition was tested by following the infiltration of leaves of the *acp1* mutants and Col-0 plants with the buffer (10 mM MgCl<sub>2</sub>), 100 μM flg22 (microbe-associated molecular patterns (MAMPs)), *Pto* DC3000 at 10<sup>8</sup> CFU/ml, and *Pto* DC3000 *hrcC*- at 10<sup>8</sup> CFU/ml. The assay was performed as described previously (Kim and Mackey, 2008). To observe the spatial patterns of the callose deposition, the infected leaves at 16 hours post-inoculation were cleared in the lactophenol and 80% ethanol for one day to bleach the chlorophyll at room temperature. Then the leaves were submerged in the aniline blue staining solution (150 mM K<sub>2</sub>HPO<sub>4</sub>, 0.01% w/v aniline blue, Cat #: 415049, Sigma-Aldrich) in the dark overnight. The leaves were mounted on the glass slides in 50% sterile glycerol for microscopic assessment. The samples were analyzed by fluorescence microscopy (Nikon Eclipse 80i epi-fluorescent microscope, Japan), using the UV excitation (327-427 nm) and the DAPI/Aniline blue emission filter (emission 417-477 nm). At least six individual leaves were applied for the analysis of each treatment. The pictures were

captured from each leaf, and the numbers of callose deposition were performed using the ImageJ software for the batch analysis (Jin and Mackey, 2017).

# H<sub>2</sub>O<sub>2</sub> Burst Assay and DAB staining for testing the H<sub>2</sub>O<sub>2</sub> accumulation.

An oxidative burst assay for testing the  $H_2O_2$  level was carried out as described previously (Wang et al., 2018) with minor modifications. The leaf discs (5mm in diameter) were cut and suspended in sterile water overnight to diminish the effects of wounds. The pre-treated leaf discs were used for the oxidative burst assay. The leaf disks were immersed in 100 ul reaction solution with the luminol substrate (Immuno-Star horseradish peroxidase substrate 170-5040, Bio-Rad),  $1.0 \,\mu$ l peroxidase (1 mg/ml), and  $1.0 \,\mu$ M flg22. After adding all the components, the samples were immediately quantified for  $H_2O_2$  production. The Luminescence was recorded continuously for 1 s at 10 s intervals for up to 30 mins with a Glomax 20/20 single well luminometer (Promega) (Park et al., 2012). Three technical replicates were applied for each treatment. The result showed the  $H_2O_2$  burst curve in real-time upon the 200 nM flg22 induction or water treatment. The related experiments had been carried out for three times with the consistent results.

According to the previous report, the staining test using 3,3-diaminobenzidine tetrahydrochloride (DAB) was also applied to detect H<sub>2</sub>O<sub>2</sub> accumulation (Xiao et al., 2003). Arabidopsis plants at the 4-week-old growth stage were sprayed with the buffer (10 mM MgCl<sub>2</sub>) or *Pto* DC3000 solution (10<sup>7</sup> CFU/ml). Around 24 hours after the treatment, the leaf samples were collected and submerged in 1mg/ml of acidic 3,3-diaminobenzidine tetrahydrochloride (DAB) solution and incubated overnight in the dark cleared using 1:1 ethanol/acetic acid clearing solution. The images were captured after the chlorophyll clearing with a light camera (Nikon) (Xiao *et al.*, 2003).

541

542

543

544

545

546

547

ACKNOWLEDGEMENTS. We greatly appreciate Arabidopsis Biological Resource Center (ABRC) for providing the Arabidopsis seeds and constructs. We gave our special thanks to Christophe Cocuron and Ana Paula Alonso from BioDiscovery Institute and the Department of Biological Sciences at the University of North Texas to help with the fatty acid level analysis. We also appreciate the help with the fatty acid analysis by Dr. Keshun Yu and Pradeep Kachroo from the Plant Pathology Department at the University of Kentucky. We are grateful to Dr. Mingzhe Shen for his help on this project.

# LITERATURE CITED

- Bashan, Y. 1997. Alternative strategies for controlling plant diseases caused by Pseudomonas
- syringae. Pages 575-583 in: Pseudomonas syringae pathovars and related pathogens,
- Springer.
- Bashan, Y., and de-Bashan, L.E. 2002. Reduction of bacterial speck (Pseudomonas syringae pv.
- tomato) of tomato by combined treatments of plant growth-promoting bacterium,
- Azospirillum brasilense, streptomycin sulfate, and chemo-thermal seed treatment.
- European Journal of Plant Pathology 108:821-829.
- Beisson, F., Li, Y., Bonaventure, G., Pollard, M., and Ohlrogge, J.B. 2007. The acyltransferase
- GPAT5 is required for the synthesis of suberin in seed coat and root of Arabidopsis. The
- 557 Plant Cell 19:351-368.
- 558 Bi, F.-C., Liu, Z., Wu, J.-X., Liang, H., Xi, X.-L., Fang, C., Sun, T.-J., Yin, J., Dai, G.-Y., and
- Rong, C. 2014. Loss of ceramide kinase in Arabidopsis impairs defenses and promotes
- ceramide accumulation and mitochondrial H2O2 bursts. The Plant Cell 26:3449-3467.
- Bonaventure, G., and Ohlrogge, J.B. 2002. Differential regulation of mRNA levels of acyl carrier
- protein isoforms in Arabidopsis. Plant physiology 128:223-235.

563 Branen, J.K., Chiou, T.-J., and Engeseth, N.J. 2001. Overexpression of acyl carrier protein-1 alters fatty acid composition of leaf tissue in Arabidopsis. Plant physiology 127:222-229. 564 Brown, A.P., Slabas, A.R., and Rafferty, J.B. 2009. Fatty acid biosynthesis in plants—metabolic 565 pathways, structure and organization. Pages 11-34 in: Lipids in photosynthesis, Springer. 566 Buttimer, C., McAuliffe, O., Ross, R.P., Hill, C., O'Mahony, J., and Coffey, A. 2017. 567 Bacteriophages and bacterial plant diseases. Frontiers in microbiology 8:34. 568 Byers, D.M., and Gong, H. 2007. Acyl carrier protein: structure-function relationships in a 569 conserved multifunctional protein family. Biochemistry and Cell Biology 85:649-662. 570 571 Chan, D.I., and Vogel, H.J. 2010. Current understanding of fatty acid biosynthesis and the acyl carrier protein. Biochemical Journal 430:1-19. 572 Chanda, B., Xia, Y., Mandal, M.K., Yu, K., Sekine, K.T., Gao, Q.M., Selote, D., Hu, Y., Stromberg, 573 574 A., Navarre, D., Kachroo, A., and Kachroo, P. 2011. Glycerol-3-phosphate is a critical mobile inducer of systemic immunity in plants. Nat Genet 43:421-427. 575 Cheng, C., Gao, X., Feng, B., Sheen, J., Shan, L., and He, P. 2013. Plant immune response to 576 pathogens differs with changing temperatures. Nat Commun 4:2530. 577 Crawford, J.M., Vagstad, A.L., Ehrlich, K.C., Udwary, D.W., and Townsend, C.A.J.C. 2008. 578 Acyl-Carrier Protein-Phosphopantetheinyltransferase Partnerships in Fungal Fatty Acid 579 Synthases 9:1559-1563. 580 Cui, H., Qiu, J., Zhou, Y., Bhandari, D.D., Zhao, C., Bautor, J., and Parker, J.E. 2018. Antagonism 581 of Transcription Factor MYC2 by EDS1/PAD4 Complexes Bolsters Salicylic Acid 582

Defense in Arabidopsis Effector-Triggered Immunity. Mol Plant 11:1053-1066.

583

- Cultrera, N.G., Alagna, F., Mariotti, R., De Marchis, F., Pompa, A., Bellucci, M., and Baldoni, L.
- 585 2014. Isolation and molecular characterization of three acyl carrier protein genes in olive
- (Olea europaea L.). Tree genetics & genomes 10:895-909.
- Dat, J., Vandenabeele, S., Vranova, E., Van Montagu, M., Inzé, D., and Van Breusegem, F. 2000.
- Dual action of the active oxygen species during plant stress responses. Cellular and
- Molecular Life Sciences CMLS 57:779-795.
- 590 Ding, P., and Ding, Y. 2020. Stories of salicylic acid: A plant defense hormone. Trends in Plant
- 591 Science.
- 592 Fan, G., Yang, Y., Li, T., Lu, W., Du, Y., Qiang, X., Wen, Q., and Shan, W. 2018. A Phytophthora
- capsici RXLR effector targets and inhibits a plant PPIase to suppress endoplasmic
- reticulum-mediated immunity. Molecular plant 11:1067-1083.
- Forcat, S., Bennett, M.H., Mansfield, J.W., and Grant, M.R. 2008. A rapid and robust method for
- simultaneously measuring changes in the phytohormones ABA, JA and SA in plants
- following biotic and abiotic stress. Plant Methods 4:16.
- Gao, Q.-M., Zhu, S., Kachroo, P., and Kachroo, A. 2015. Signal regulators of systemic acquired
- resistance. Frontiers in plant science 6:228.
- 600 Gao, Q.M., Yu, K., Xia, Y., Shine, M.B., Wang, C., Navarre, D., Kachroo, A., and Kachroo, P.
- 601 2014. Mono- and digalactosyldiacylglycerol lipids function nonredundantly to regulate
- systemic acquired resistance in plants. Cell Rep 9:1681-1691.
- 603 Gautam, J.K., Giri, M.K., Singh, D., Chattopadhyay, S., and Nandi, A.K. 2021. MYC2 influences
- salicylic acid biosynthesis and defense against bacterial pathogens in Arabidopsis thaliana.
- 605 Physiol Plant 173:2248-2261.

606 Geng, X., Jin, L., Shimada, M., Kim, M.G., and Mackey, D. 2014. The phytotoxin coronatine is a multifunctional component of the virulence armament of Pseudomonas syringae. Planta 607 240:1149-1165. 608 Gimenez-Ibanez, S., Boter, M., Fernández-Barbero, G., Chini, A., Rathjen, J.P., and Solano, R. 609 2014. The bacterial effector HopX1 targets JAZ transcriptional repressors to activate 610 jasmonate signaling and promote infection in Arabidopsis. PLoS biology 12. 611 Guo, W., Zuo, Z., Cheng, X., Sun, J., Li, H., Li, L., and Qiu, J.L. 2014. The chloride channel 612 family gene CLCd negatively regulates pathogen-associated molecular pattern (PAMP)-613 triggered immunity in Arabidopsis. J Exp Bot 65:1205-1215. 614 Gupta, A., Bhardwaj, M., and Tran, L.P. 2020. Jasmonic Acid at the Crossroads of Plant Immunity 615 and Pseudomonas syringae Virulence. Int J Mol Sci 21. 616 617 Hansen, L., and von Wettstein-Knowles, P. 1991. The barley genes Acl1 and Acl3 encoding acyl carrier proteins I and III are located on different chromosomes. Molecular and General 618 Genetics MGG 229:467-478. 619 Hirt, H. 2016. Aguaporins link ROS signaling to plant immunity. Plant physiology 171:1540-1540. 620 Hloušek-Radojčić, A., Post-Beittenmiller, D., and Ohlrogge, J.B. 1992. Expression of constitutive 621 and tissue-specific acyl carrier protein isoforms in Arabidopsis. Plant physiology 98:206-622 214. 623 Huang, J., Xue, C., Wang, H., Wang, L., Schmidt, W., Shen, R., and Lan, P. 2017. Genes of ACYL 624 CARRIER PROTEIN family show different expression profiles and overexpression of 625 ACYL CARRIER PROTEIN 5 modulates fatty acid composition and enhances salt stress 626 tolerance in Arabidopsis. Frontiers in plant science 8:987. 627

- 628 Huang, L.Q., Chen, D.K., Li, P.P., Bao, H.N., Liu, H.Z., Yin, J., Zeng, H.Y., Yang, Y.B., Li, Y.K.,
- Xiao, S., and Yao, N. 2021. Jasmonates modulate sphingolipid metabolism and accelerate
- cell death in the ceramide kinase mutant acd5. Plant Physiol 187:1713-1727.
- Jiang, S., Yao, J., Ma, K.-W., Zhou, H., Song, J., He, S.Y., and Ma, W. 2013. Bacterial effector
- activates jasmonate signaling by directly targeting JAZ transcriptional repressors. PLoS
- pathogens 9.
- Jin, L., and Mackey, D.M. 2017. Measuring callose deposition, an indicator of cell wall
- reinforcement, during bacterial infection in Arabidopsis. Pages 195-205 in: Plant Pattern
- Recognition Receptors, Springer.
- Jones, J.D., and Dangl, J.L. 2006. The plant immune system. nature 444:323-329.
- Jones, J.D., Vance, R.E., and Dangl, J.L. 2016. Intracellular innate immune surveillance devices
- in plants and animals. Science 354:aaf6395.
- Jung, H.W., Tschaplinski, T.J., Wang, L., Glazebrook, J., and Greenberg, J.T. 2009. Priming in
- systemic plant immunity. Science 324:89-91.
- Kachroo, A., Lapchyk, L., Fukushige, H., Hildebrand, D., Klessig, D., and Kachroo, P. 2003.
- Plastidial fatty acid signaling modulates salicylic acid-and jasmonic acid-mediated
- defense pathways in the Arabidopsis ssi2 mutant. The Plant Cell 15:2952-2965.
- Kachroo, P., Shanklin, J., Shah, J., Whittle, E.J., and Klessig, D.F. 2001. A fatty acid desaturase
- modulates the activation of defense signaling pathways in plants. Proceedings of the
- National Academy of Sciences 98:9448-9453.
- Kim, M.G., and Mackey, D. 2008. Measuring cell-wall-based defenses and their effect on bacterial
- growth in Arabidopsis. Pages 443-452 in: Innate Immunity, Springer.

- Kim, M.G., Da Cunha, L., McFall, A.J., Belkhadir, Y., DebRoy, S., Dangl, J.L., and Mackey, D.
- 651 2005. Two Pseudomonas syringae type III effectors inhibit RIN4-regulated basal defense
- in Arabidopsis. Cell 121:749-759.
- Kim, Y., Tsuda, K., Igarashi, D., Hillmer, R.A., Sakakibara, H., Myers, C.L., and Katagiri, F.
- 654 2014. Mechanisms underlying robustness and tunability in a plant immune signaling
- network. Cell host & microbe 15:84-94.
- Kwak, J.M., Nguyen, V., and Schroeder, J.I. 2006. The role of reactive oxygen species in hormonal
- responses. Plant Physiology 141:323-329.
- Lan, P., Li, W., and Schmidt, W. 2012. Complementary proteome and transcriptome profiling in
- phosphate-deficient Arabidopsis roots reveals multiple levels of gene regulation.
- Molecular & Cellular Proteomics 11:1156-1166.
- Laurie-Berry, N., Joardar, V., Street, I.H., and Kunkel, B.N. 2006. The Arabidopsis thaliana
- JASMONATE INSENSITIVE 1 gene is required for suppression of salicylic acid-
- dependent defenses during infection by Pseudomonas syringae. Molecular Plant-Microbe
- Interactions 19:789-800.
- 665 Li, J., Yin, J., Wu, J.X., Wang, L.Y., Liu, Y., Huang, L.Q., Wang, R.H., and Yao, N. 2021.
- Ceramides regulate defense response by binding to RbohD in Arabidopsis. Plant J.
- 667 Li, N., Han, X., Feng, D., Yuan, D., and Huang, L.-J. 2019. Signaling Crosstalk between Salicylic
- Acid and Ethylene/Jasmonate in Plant Defense: Do We Understand What They Are
- Whispering? International Journal of Molecular Sciences 20.
- 670 Lim, G.-H., Liu, H., Yu, K., Liu, R., Shine, M.B., Fernandez, J., Burch-Smith, T., Mobley, J.K.,
- McLetchie, N., Kachroo, A., and Kachroo, P. 2020. The plant cuticle regulates apoplastic
- transport of salicylic acid during systemic acquired resistance 6:eaaz0478.

- Liu, H., and Timko, M.P. 2021. Jasmonic Acid Signaling and Molecular Crosstalk with Other 673
- Phytohormones. Int J Mol Sci 22. 674
- Liu, J., Elmore, J.M., Fuglsang, A.T., Palmgren, M.G., Staskawicz, B.J., and Coaker, G. 2009. 675
- RIN4 functions with plasma membrane H+-ATPases to regulate stomatal apertures during 676
- pathogen attack. PLoS biology 7. 677
- Liu, Y.-H., Offler, C.E., and Ruan, Y.-L. 2014. A simple, rapid, and reliable protocol to localize 678
- hydrogen peroxide in large plant organs by DAB-mediated tissue printing. Frontiers in 679
- plant science 5:745. 680
- Lolle, S.J., Berlyn, G.P., Engstrom, E.M., Krolikowski, K.A., Reiter, W.-D., and Pruitt, R.E. 1997. 681
- Developmental Regulation of Cell Interactions in the Arabidopsis fiddlehead-1 Mutant: A 682
- Role for the Epidermal Cell Wall and Cuticle. Developmental biology 189:311-321. 683
- Luna, E., Pastor, V., Robert, J., Flors, V., Mauch-Mani, B., and Ton, J. 2011. Callose deposition: 684
- a multifaceted plant defense response. Molecular Plant-Microbe Interactions 24:183-193. 685
- Maejima, E., Watanabe, T., Osaki, M., and Wagatsuma, T. 2014. Phosphorus deficiency enhances 686
- aluminum tolerance of rice (Oryza sativa) by changing the physicochemical characteristics 687
- of root plasma membranes and cell walls. Journal of plant physiology 171:9-15. 688
- Malinovsky, F.G., Fangel, J.U., and Willats, W.G. 2014. The role of the cell wall in plant immunity. 689
- Frontiers in plant science 5:178. 690
- Marrakchi, H., Zhang, Y.-M., and Rock, C. (2002). Mechanistic diversity and regulation of Type 691
- 692 II fatty acid synthesis (Portland Press Ltd.).
- Mata-Pérez, C., Sánchez-Calvo, B., Begara-Morales, J.C., Luque, F., Jiménez-Ruiz, J., Padilla, 693
- M.N., Fierro-Risco, J., Valderrama, R., Fernández-Ocaña, A., and Corpas, F.J. 2015. 694

Transcriptomic profiling of linolenic acid-responsive genes in ROS signaling from RNA-695 seq data in Arabidopsis. Frontiers in plant science 6:122. 696 Meier, J.L., Haushalter, R.W., and Burkart, M.D. 2010. A mechanism based protein crosslinker 697 for acyl carrier protein dehydratases. Bioorganic & medicinal chemistry letters 20:4936-698 4939. 699 Melotto, M., Underwood, W., Koczan, J., Nomura, K., and He, S.Y. 2006. Plant stomata function 700 in innate immunity against bacterial invasion. Cell 126:969-980. 701 Meyer, E.H., Heazlewood, J.L., and Millar, A.H. 2007. Mitochondrial acyl carrier proteins in 702 703 Arabidopsis thaliana are predominantly soluble matrix proteins and none can be confirmed as subunits of respiratory Complex I. Plant molecular biology 64:319-327. 704 Mittler, R., Vanderauwera, S., Gollery, M., and Van Breusegem, F. 2004. Reactive oxygen gene 705 706 network of plants. Trends in plant science 9:490-498. Montillet, J.-L., Leonhardt, N., Mondy, S., Tranchimand, S., Rumeau, D., Boudsocq, M., Garcia, 707 A.V., Douki, T., Bigeard, J., and Lauriere, C. 2013. An abscisic acid-independent oxylipin 708 pathway controls stomatal closure and immune defense in Arabidopsis. PLoS biology 11. 709 Mueller, M.J., Brodschelm, W., Spannagl, E., and Zenk, M.H.J.P.o.t.N.A.o.S. 1993. Signaling in 710 the elicitation process is mediated through the octadecanoid pathway leading to jasmonic 711 acid 90:7490-7494. 712 Nelson, B.K., Cai, X., and Nebenführ, A. 2007. A multicolored set of in vivo organelle markers 713 714 for co-localization studies in Arabidopsis and other plants. The Plant Journal 51:1126-1136. Ngou, B.P.M., Ahn, H.K., Ding, P., and Jones, J.D.G. 2021. Mutual potentiation of plant immunity 715 by cell-surface and intracellular receptors. Nature 592:110-115. 716

Ohlrogge, J.B., and Kuo, T.M. 1985. Plants have isoforms for acyl carrier protein that are 717 expressed differently in different tissues. Journal of Biological Chemistry 260:8032-8037. 718 Ohlrogge, J.B., Kuhn, D.N., and Stumpf, P. 1979. Subcellular localization of acyl carrier protein 719 720 in leaf protoplasts of Spinacia oleracea. Proceedings of the National Academy of Sciences 76:1194-1198. 721 Park, C.-H., Chen, S., Shirsekar, G., Zhou, B., Khang, C.H., Songkumarn, P., Afzal, A.J., Ning, 722 Y., Wang, R., and Bellizzi, M. 2012. The Magnaporthe oryzae effector AvrPiz-t targets the 723 RING E3 ubiquitin ligase APIP6 to suppress pathogen-associated molecular pattern-724 triggered immunity in rice. The plant cell 24:4748-4762. 725 Peng, Q., Wang, Z., Liu, P., Liang, Y., Zhao, Z., Li, W., Liu, X., and Xia, Y. 2020. Oxathiapiprolin, 726 a novel chemical inducer activates the plant disease resistance. International journal of 727 728 molecular sciences 21:1223. Pieterse, C.M., Van der Does, D., Zamioudis, C., Leon-Reyes, A., and Van Wees, S.C. 2012. 729 Hormonal modulation of plant immunity. Annual review of cell and developmental biology 730 28:489-521. 731 Prost, I., Dhondt, S., Rothe, G., Vicente, J., Rodriguez, M.J., Kift, N., Carbonne, F., Griffiths, G., 732 Esquerré-Tugayé, M.-T., and Rosahl, S. 2005. Evaluation of the antimicrobial activities of 733 plant oxylipins supports their involvement in defense against pathogens. Plant physiology 734 139:1902-1913. 735 Rossi, L., Escudero, J., Hohn, B., and Tinland, B. 1993. Efficient and sensitive assay for T-DNA-736

dependent transient gene expression. Plant Molecular Biology Reporter 11:220-229.

- Roujeinikova, A., Baldock, C., Simon, W.J., Gilroy, J., Baker, P.J., Stuitje, A.R., Rice, D.W.,
- Slabas, A.R., and Rafferty, J.B.J.S. 2002. X-ray crystallographic studies on butyryl-ACP
- reveal flexibility of the structure around a putative acyl chain binding site 10:825-835.
- Ruan, J., Zhou, Y., Zhou, M., Yan, J., Khurshid, M., Weng, W., Cheng, J., and Zhang, K. 2019.
- Jasmonic acid signaling pathway in plants. International journal of molecular sciences
- 743 20:2479.
- Ruuska, S.A., Girke, T., Benning, C., and Ohlrogge, J.B. 2002. Contrapuntal networks of gene
- expression during Arabidopsis seed filling. The Plant Cell 14:1191-1206.
- SAFFORD, R., WINDUST, J.H., LUCAS, C., DE SILVA, J., JAMES, C.M., HELLYER, A.,
- SMITH, C.G., SLABAS, A.R., and HUGHES, S.G. 1988. Plastid-localised seed
- acyl-carrier protein of Brassica napus is encoded by a distinct, nuclear multigene family.
- European journal of biochemistry 174:287-295.
- Santino, A., Taurino, M., De Domenico, S., Bonsegna, S., Poltronieri, P., Pastor, V., and Flors, V.
- 751 2013. Jasmonate signaling in plant development and defense response to multiple (a)biotic
- 752 stresses. Plant Cell Rep 32:1085-1098.
- 753 Shirasu, K., Nakajima, H., Rajasekhar, V.K., Dixon, R.A., and Lamb, C. 1997. Salicylic acid
- potentiates an agonist-dependent gain control that amplifies pathogen signals in the
- activation of defense mechanisms. The Plant Cell 9:261-270.
- Song, P., and Allen, R.D. 1997. Identification of a cotton fiber-specific acyl carrier protein cDNA
- by differential display. Biochimica et Biophysica Acta (BBA)-Gene Structure and
- 758 Expression 1351:305-312.
- Spoel, S.H., and Dong, X. 2012. How do plants achieve immunity? Defence without specialized
- immune cells. Nature reviews immunology 12:89-100.

- Takemoto, D., and Jones, D.A. 2005. Membrane release and destabilization of Arabidopsis RIN4
- following cleavage by Pseudomonas syringae AvrRpt2. Molecular plant-microbe
- 763 interactions 18:1258-1268.
- Vlot, A.C., Dempsey, D.M.A., and Klessig, D.F. 2009. Salicylic acid, a multifaceted hormone to
- combat disease. Annual review of phytopathology 47:177-206.
- Wang, C., El-Shetehy, M., Shine, M., Yu, K., Navarre, D., Wendehenne, D., Kachroo, A., and
- Kachroo, P. 2014. Free radicals mediate systemic acquired resistance. Cell Reports 7:348-
- 768 355.
- Wang, M., Rui, L., Yan, H., Shi, H., Zhao, W., Lin, J.E., Zhang, K., Blakeslee, J.J., Mackey, D.,
- and Tang, D. 2018. The major leaf ferredoxin Fd2 regulates plant innate immunity in
- Arabidopsis. Molecular plant pathology 19:1377-1390.
- 772 Wang, Q., Zhu, B., Chen, C., Yuan, Z., Guo, J., Yang, X., Wang, S., Lv, Y., Liu, Q., Yang, B.,
- Sun, C., Wang, P., and Deng, X. 2021. A Single Nucleotide Substitution of GSAM Gene
- Causes Massive Accumulation of Glutamate 1-Semialdehyde and Yellow Leaf Phenotype
- 775 in Rice. Rice (N Y) 14:50.
- Wasternack, C., and Strnad, M. 2019. Jasmonates are signals in the biosynthesis of secondary
- metabolites—Pathways, transcription factors and applied aspects—A brief review. New
- 5778 biotechnology 48:1-11.
- 779 Wu, J.X., Li, J., Liu, Z., Yin, J., Chang, Z.Y., Rong, C., Wu, J.L., Bi, F.C., and Yao, N. 2015. The
- Arabidopsis ceramidase At ACER functions in disease resistance and salt tolerance. The
- 781 Plant Journal 81:767-780.

- Xia, Y., Yu, K., Gao, Q.-m., Wilson, E., Navarre, D., Kachroo, P., and Kachroo, A. 2012. Acyl
- CoA binding proteins are required for cuticle formation and plant responses to microbes.
- Frontiers in plant science 3:224.
- Xia, Y., Gao, Q.-M., Yu, K., Lapchyk, L., Navarre, D., Hildebrand, D., Kachroo, A., and Kachroo,
- P. 2009. An intact cuticle in distal tissues is essential for the induction of systemic acquired
- resistance in plants. Cell Host & Microbe 5:151-165.
- Xiao, S., Brown, S., Patrick, E., Brearley, C., and Turner, J.G. 2003. Enhanced transcription of the
- Arabidopsis disease resistance genes RPW8. 1 and RPW8. 2 via a salicylic acid–dependent
- amplification circuit is required for hypersensitive cell death. The Plant Cell 15:33-45.
- Xin, X.-F., and He, S.Y. 2013. Pseudomonas syringae pv. tomato DC3000: a model pathogen for
- probing disease susceptibility and hormone signaling in plants. Annual review of
- 793 phytopathology 51:473-498.
- Xin, X.-F., Kvitko, B., and He, S.Y. 2018. Pseudomonas syringae: what it takes to be a pathogen.
- Nature Reviews Microbiology 16:316.
- Yang, J., Duan, G., Li, C., Liu, L., Han, G., Zhang, Y., and Wang, C. 2019. The Crosstalks
- 797 Between Jasmonic Acid and Other Plant Hormone Signaling Highlight the Involvement of
- Jasmonic Acid as a Core Component in Plant Response to Biotic and Abiotic Stresses.
- Frontiers in plant science 10.
- Yi, S.Y., Shirasu, K., Moon, J.S., Lee, S.-G., and Kwon, S.-Y. 2014. The activated SA and JA
- signaling pathways have an influence on flg22-triggered oxidative burst and callose
- deposition. PloS one 9.
- Yu, K., Soares, J.M., Mandal, M.K., Wang, C., Chanda, B., Gifford, A.N., Fowler, J.S., Navarre,
- D., Kachroo, A., and Kachroo, P. 2013. A feedback regulatory loop between G3P and lipid

805	transfer proteins DIR1 and AZI1 mediates azelaic-acid-induced systemic immunity. Cell
806	Reports 3:1266-1278.
807	Yuan, M., Ngou, B.P.M., Ding, P., and Xin, X.F. 2021a. PTI-ETI crosstalk: an integrative view of
808	plant immunity. Curr Opin Plant Biol 62:102030.
809	Yuan, M., Jiang, Z., Bi, G., Nomura, K., Liu, M., Wang, Y., Cai, B., Zhou, J.M., He, S.Y., and
810	Xin, X.F. 2021b. Pattern-recognition receptors are required for NLR-mediated plant
811	immunity. Nature 592:105-109.
812	Zhao, Z., Yang, X., Lü, S., Fan, J., Opiyo, S., Yang, P., Mangold, J., Mackey, D., and Xia, Y.
813	2020. Deciphering the novel role of AtMIN7 in cuticle formation and defense against the
814	bacterial pathogen infection. International journal of molecular sciences 21:5547.
815	Zheng, Xy., Spivey, N.W., Zeng, W., Liu, PP., Fu, Z.Q., Klessig, D.F., He, S.Y., and Dong, X.
816	2012. Coronatine promotes Pseudomonas syringae virulence in plants by activating a
817	signaling cascade that inhibits salicylic acid accumulation. Cell host & microbe 11:587-
818	596.
819	Zoeller, M., Stingl, N., Krischke, M., Fekete, A., Waller, F., Berger, S., and Mueller, M.J. 2012.
820	Lipid profiling of the Arabidopsis hypersensitive response reveals specific lipid
821	peroxidation and fragmentation processes: biogenesis of pimelic and azelaic acid. Plant
822	Physiol 160:365-378.
823	
024	
824	
825	
826	

Figure captions

827

828

829

830

831

832

833

834

835

836

837

838

839

840

841

842

843

844

845

846

847

848

Figure 1. Characterization of the ACPs family and identification of acp1 mutants. (a) The conserved domains of Arabidopsis Acyl Carrier Proteins (ACPs). Image modified from National Center for Biotechnology Information (NCBI). (b) Phylogenetic analyses of Arabidopsis ACP protein family members. Protein sequences are aligned by Clustal Omega. The Phylogenetic Tree was constructed from Simple Phylogeny via EMBL-EBI. The numbers shown indicated the distance values, which were the length of the branch immediately leading to the node. (c) Relative gene expression of ACP1 in WT and acp1 mutants and normalized to the expression of ACTIN. Data represent means  $\pm$  SE (n = 4), which are from one of the three independent repeats with consistent results. Significant differences between the WT and acp1 mutants were indicated by the asterisks determined from the Student's *t*-test (p < 0.05). Figure 2. The visualization of subcellular localization of ACP1 in the transiently transformed Nicotiana benthamiana. (a) GFP signals of the ACP1-GFP fusion protein. (b) GFP signals of the empty vector pYBA1122-35S-GFP. Green fluorescence indicates GFP signal; red fluorescence indicates plastid autofluorescence; yellow fluorescence shows the merged images with two types of fluorescence. The signals of ACP1-GFP and PT-mCherry were overlapped to the exact localization at the plastids. Scale bar =25  $\mu$ m. Figure 3. The responses of WT and acp1 mutant plants to the bacterial pathogen Pto DC3000 **infection.** (a) Plant phenotypes of WT Col-0 and the *acp1* mutants in response to the *Pto* pathogen infection. WT Col-0, acp1-1, and acp1-2 plant leaves were syringe infiltrated with 5×10<sup>5</sup> CFU/mL of Pto DC3000. Images were captured three days post-infiltration. (b) Bacterial multiplication in the leaves of WT and acp1 mutants at 0 and 3 days after the inoculation. Data represent means  $\pm$ 

850

851

852

853

854

855

856

857

858

859

860

861

862

863

864

865

866

867

868

869

870

871

SE (n = 4), which are from one of the three independent repeats with consistent results. Different letters a-c within the figure indicate the significant differences at p < 0.05, which was calculated by one-way analysis of variance (ANOVA) using SPSS ver. 21. (c) Relative PTI marker gene expressions in WT and acp1 mutants plant leaves at 0, 6, and 48 hours after the inoculation with  $5\times10^5$  CFU/mL of *Pto* DC3000. The gene expression was quantified by qPCR and normalized to the expression of *UBIOUITIN*. The experiments were repeated three times with similar results. Data represent means  $\pm$  SE (n = 4). Significant differences between the WT and *acp1* mutants were indicated by the asterisks determined from the Student's *t*-test (p < 0.05). Figure 4. The levels of FAs in the 4-week-old WT and acp1 mutant plant leaves. (a) The abundance of the FAs at 4-week-old *acp1* mutants and WT plant leaves without any treatment. Data represent means  $\pm$  SE (n = 4), which are from one of the three independent repeats with consistent results. Significant differences between the WT and acp1 mutants were indicated by the asterisks determined from the Student's t-test (p < 0.05). (b) The abundance of C18:3 FAs at 4week-old acp1 mutants and WT plant leaves 48 hours after the Pto DC3000 and buffer MgCl<sub>2</sub> inoculation. The FA analysis was extracted by placing leaf tissues in 2 ml of 3% H<sub>2</sub>SO<sub>4</sub> in methanol with 17:0 FA as the standard. Data represent means  $\pm$  SE (n = 4), which are from one of the three independent repeats with consistent results. Different letters a-c within the figure indicate the significant differences at p < 0.05, which was calculated by one-way analysis of variance (ANOVA) using SPSS ver. 21. Figure 5. The acp1 mutants accumulated a higher level of salicylic acid (SA) and a lower level of jasmonic acid (JA) after the pathogen Pto DC3000 infection. WT and acp1 mutant plants were inoculated with the buffer (10 mM MgCl<sub>2</sub>) or Pto DC3000 at 5×10<sup>5</sup> CFU/ml by leaf infiltration. Leaf samples were collected for quantification of free JA (a) and JA-Ile/Leu (JA-

isoleucine/leucine) (b), free SA (c), and SAG (SA-glycoside) (d) at 48 hours post-inoculation. Data 872 represent means  $\pm$  SE (n = 4), which are from one of the three independent repeats with consistent 873 results. Different letters a-c within the figure (a-d) indicate the significant differences at p < 0.05, 874 which was calculated by one-way analysis of variance (ANOVA) using SPSS ver. 21. 875 Figure 6. The acp1 mutants showed the enhanced SA-related gene expression and reduced 876 877 JA-related gene expression after the Pto DC3000 treatment. After the inoculation with Pto DC3000 at 5×10<sup>5</sup> CFU/ml by infiltration, the total RNA was extracted from the inoculated leaves 878 of WT Col-0 and acp1 mutants at the indicated times. The relative transcriptional levels of SID2 879 880 (a), PR1 (b), PDF1.2 (c), COII (d), and MYC2 (e) were determined by qPCR with UBIQUITIN as the internal reference gene. Data represent means  $\pm$  SE (n = 4), which are from one of the three 881 independent repeats with consistent results. Significant differences between the WT and acp1 882 mutants were indicated by the asterisks determined from the Student's *t*-test (p < 0.05). 883 Figure 7. Effects of MeJA and C18:3 FA (linolenic acid) treatments on the plant defense of 884 acp1 mutants against Pto DC3000. Four-week-old WT Col-0 and acp1 plants were sprayed with 885 solvent control (0.1% ethanol) or 50 µM MeJA or 0.1 mM linolenic acid. Plants were syringe 886 infiltrated with 5×10<sup>5</sup> CFU/mL of Pto DC3000 24 hours after treatments. The bacterial 887 888 multiplication in the leaves of WT and acp mutants was checked three days after the inoculation (a &b). Data represent means  $\pm$  SE (n = 4), which are from one of three independent repeats with 889 consistent results. Different letters a-c within the figures indicate the significant differences at p < 1890 0.05, calculated by one-way analysis of variance (ANOVA) using SPSS ver. 21. 891 Figure 8. The acp1 mutants showed the enhanced H<sub>2</sub>O<sub>2</sub> accumulation upon the MAMP flg22 892 893 treatment or *Pto* DC3000 inoculation (a). The real-time chemiluminescence of H<sub>2</sub>O<sub>2</sub> burst curve

upon the 100 nM flg22 induction or water treatment. Leaf discs (5 mm in diameter) were pretreated with water overnight. Pre-treated leaf discs were treated with 100 nM flg22 in the buffer, which contained the luminol and horseradish peroxidase or mock treatment (water). Luminescence was recorded for 30 mins using the GLOMAX luminometer. Data represent means  $\pm$  SE (n = 5), which are from one of the two independent repeats with consistent results. (b). WT Col-0 and *acp1* mutant plants were sprayed with *Pto* DC3000 (10<sup>7</sup> CFU/ml) or with buffer (10 mM MgCl<sub>2</sub>) as the control. The H<sub>2</sub>O<sub>2</sub> production was visualized by the 3,3-diaminobenzidine tetrahydrochloride (DAB) staining at 48 hours post-inoculation. The brown color indicated the H<sub>2</sub>O<sub>2</sub> production site. (c) The production of H<sub>2</sub>O<sub>2</sub> upon *Pto* DC3000 infection and buffer treatment is indicated by the DAB staining intensity. Data represent means  $\pm$  SE (n = 3), which are from one of the three independent repeats with consistent results. Significant differences between the WT and *acp1* mutants were indicated by the asterisks determined from the Student's *t*-test (p < 0.05).

Figure 9. The *acp1* mutants showed the enhanced callose deposition in response to the MAMP treatment and the pathogen *Pto* infection. The leaves of *acp1* mutants and WT Col-0 plants were infiltrated with the buffer (10 mM MgCl<sub>2</sub>), 100  $\mu$ M flg22, *Pto* DC3000 at 10<sup>8</sup> CFU/ml, and *Pto* DC3000 *hrcC*- at 10<sup>8</sup> CFU/ml. Callose deposition quantification was determined by staining the leaves with 0.01% aniline blue solution 16 hours after inoculation. (a). The images of callose deposition in Arabidopsis leaves. (b). The number of callose deposition points was quantified by Image J software. The numbers shown are mean callose deposits per mm<sup>2</sup> from six images. Data represent means  $\pm$  SE (n = 12), which are from one of the three independent repeats with consistent results. Significant differences between the *acp1* mutants and WT were indicated by the asterisks determined from the Student's *t*-test (p < 0.05).

**Figure S1.** The relative transcriptional levels of ACPs in response to the bacterial pathogen Pto 918 919 DC3000 infection. Col-0 leaves were infiltrated with buffer and 5×10<sup>5</sup> CFU/mL of *Pto* DC3000. 920 Quantitative real-time PCR (qPCR) was used to measure the amount of ACPs transcript (relative to ACTIN) at 6 hours post-inoculation. Data represent means  $\pm$  SE (n = 4), which are from one of 921 922 the three independent repeats with consistent results. Significant differences between the WT and acp1 mutants were indicated by the asterisks determined from the Student's t-test (p < 0.05). 923 Figure S2. The diagram of the ACP1 genomic structure and T-DNA insertion sites in two 924 acp1 mutants. The position and orientation of primers used for PCR confirmation of the acp1-925 1 (F1 and R1) and acp1-2 mutants (F2 and R2) are marked by arrows. LBa1.3 and LB3 (left border 926 primer) are specific for the T-DNA sequence of acp1-1 and acp1-2 mutants, respectively. The 927 position and orientation of primers used for qRT-PCR are indicated as qPCRF and qPCRR. 928 Figure S3. The physiological parameters of the acp1 mutants and WT plants. (a). Plant 929 biomass (weight) of the acp1 mutants and WT plants. (b). Plant height of the acp1 mutants and 930 WT plants. Data represent means  $\pm$  SE (n = 4), which are from one of the two independent repeats 931 with consistent results. Significant differences between the acp1 mutants and WT were indicated 932 by the asterisks determined from the Student's t-test (p < 0.05). NS represents no significance. (c). 933 Morphological phenotypes of rosettes from 4-week-old acp1 mutants and WT plants. (d). 934

**Supporting Information figure captions** 

917

935

936

937

938

Figure S4. Chlorophyll content and chlorophyll leaching rate of WT plant leaves (blue circles), *acp1-1* mutant (orange circles), and *acp1-2* mutant (grey circles). The *acp1* mutants showed similar chlorophyll content and chlorophyll leaching rate to the WT Col-0. Data represent

Morphological phenotypes of the 6-week-old *acp1* mutants and WT plants.

939	means $\pm$ SE (n = 3), which are from one of the three independent repeats with consistent results.
940	Significant differences between the $acp1$ mutants and WT were indicated by the asterisks
941	determined from the Student's <i>t</i> -test ( $p < 0.05$ ).
942	Figure S5. Basal transcript levels of JA-related genes in 4-week-old acp1 mutants and WT
943	plant leaves. The JA biosynthesis genes LOX3, AOS, and JA downstream signaling genes JAZ1
944	and $\it JAZ10$ were quantified by qRT-PCR and normalized to the expression of $\it UBIQUITIN$ . Data
945	represent means $\pm$ SE (n = 4), which are from one of the three independent repeats with consistent
946	results. Significant differences between the WT and $acp1$ mutants were indicated by the asterisks
947	determined from the Student's <i>t</i> -test ( $p < 0.05$ ).
948	Figure S6. The ACP1 gene expressions in different tissues of Arabidopsis plants. The ACP1
949	gene expression at different tissues of the Arabidopsis plant is shown in different colors. Related
950	information is obtained from Arabidopsis eFP Browser. http://bar.utoronto.ca/eplant/.
951	Table S1. The accession number list of ACP1 homologs
952	Table S2. The primer list for the PCR and RT-qPCR

#### Figure 1.

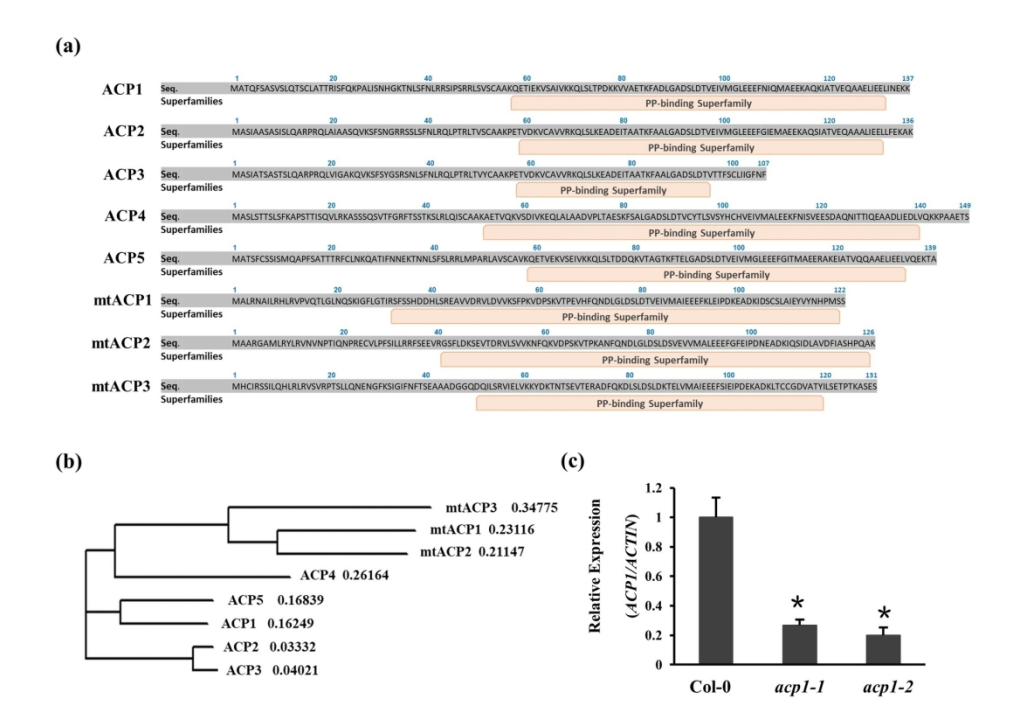


Figure 1. Characterization of the ACPs family and identification of acp1 mutants. (a) The conserved domains of Arabidopsis Acyl Carrier Proteins (ACPs). Image modified from National Center for Biotechnology Information (NCBI). (b) Phylogenetic analyses of Arabidopsis ACP protein family members. Protein sequences are aligned by Clustal Omega. The Phylogenetic Tree was constructed from Simple Phylogeny via EMBL-EBI. The numbers shown indicated the distance values, which were the length of the branch immediately leading to the node. (c) Relative gene expression of ACP1 in WT and acp1 mutants and normalized to the expression of ACTIN. Data represent means  $\pm$  SE (n = 4), which are from one of the three independent repeats with consistent results. Significant differences between the WT and acp1 mutants were indicated by the asterisks determined from the Student's t-test (p < 0.05).

176x138mm (300 x 300 DPI)

Figure 2.

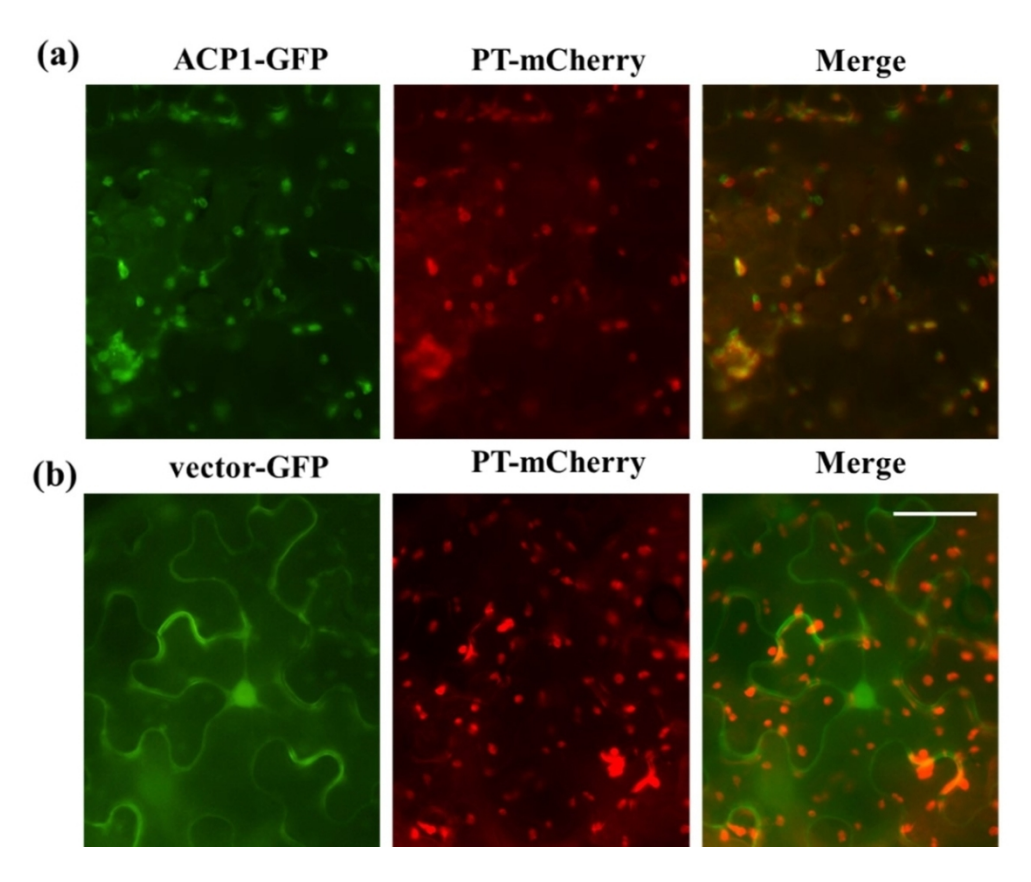


Figure 2. The visualization of subcellular localization of ACP1 in the transiently transformed *Nicotiana benthamiana*. (a) GFP signals of the ACP1-GFP fusion protein. (b) GFP signals of the empty vector pYBA1122-35S-GFP. Green fluorescence indicates GFP signal; red fluorescence indicates plastid autofluorescence; yellow fluorescence shows the merged images with two types of fluorescence. The signals of ACP1-GFP and PT-mCherry were overlapped to the exact localization at the plastids. Scale bar =25 μm.

101x97mm (300 x 300 DPI)

Figure 3.

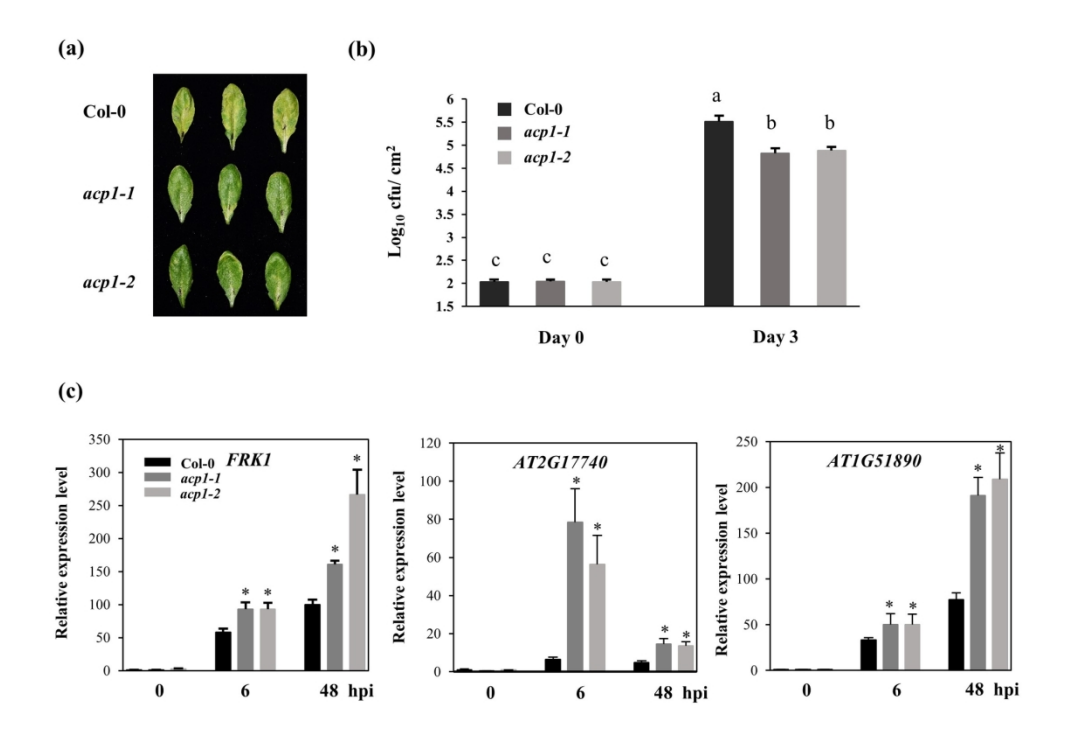
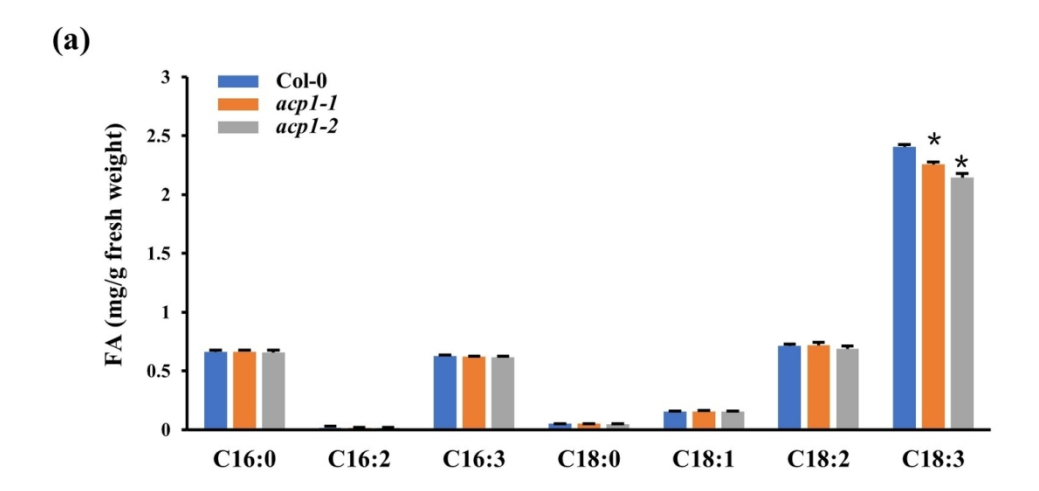


Figure 3. The responses of WT and acp1 mutant plants to the bacterial pathogen Pto DC3000 infection. (a) Plant phenotypes of WT Col-0 and the acp1 mutants in response to the Pto pathogen infection. WT Col-0, acp1-1, and acp1-2 plant leaves were syringe infiltrated with  $5\times10^5$  CFU/mL of Pto DC3000. Images were captured three days post- infiltration. (b) Bacterial multiplication in the leaves of WT and acp mutants at 0 and 3 days after the inoculation. Data represent means  $\pm$  SE (n = 4), which are from one of the three independent repeats with consistent results. Different letters a-c within the figure indicate the significant differences at p < 0.05, which was calculated by one-way analysis of variance (ANOVA) using SPSS ver. 21. (c) Relative PTI marker gene expressions in WT and acp1 mutants plant leaves at 0, 6, and 48 hours after the inoculation with  $5\times10^5$  CFU/mL of Pto DC3000. The gene expression was quantified by qPCR and normalized to the expression of UBIQUITIN. The experiments were repeated three times with similar results. Data represent means  $\pm$  SE (n = 4). Significant differences between the WT and acp1 mutants were indicated by the asterisks determined from the Student's t-test (p < 0.05).

169x135mm (300 x 300 DPI)

Figure 4.



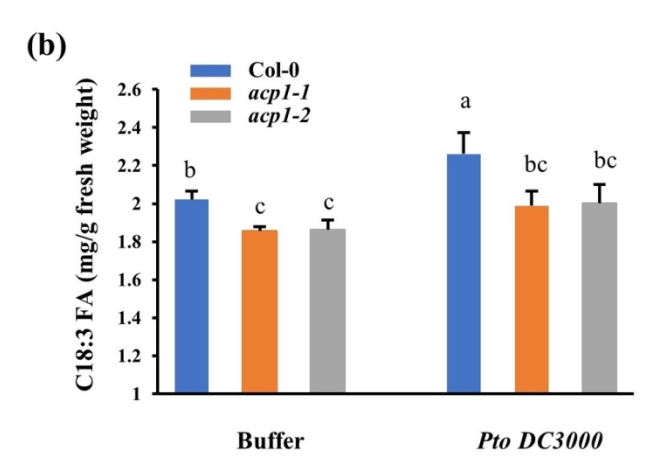


Figure 4. The levels of FAs in the 4-week-old WT and acp1 mutant plant leaves. (a) The abundance of the FAs at 4-week-old acp1 mutants and WT plant leaves without any treatment. Data represent means  $\pm$  SE (n = 4), which are from one of the three independent repeats with consistent results. Significant differences between the WT and acp1 mutants were indicated by the asterisks determined from the Student's t-test (p < 0.05). (b) The abundance of C18:3 FAs at 4-week-old acp1 mutants and WT plant leaves 48 hours after the Pto DC3000 and buffer MgCl $_2$  inoculation. The FA analysis was extracted by placing leaf tissues in 2 ml of 3% H $_2$ SO $_4$  in methanol with 17:0 FA as the standard. Data represent means  $\pm$  SE (n = 4), which are from one of the three independent repeats with consistent results. Different letters a-c within the figure indicate the significant differences at p < 0.05, which was calculated by one-way analysis of variance (ANOVA) using SPSS ver. 21.

127x139mm (300 x 300 DPI)

Figure 5.

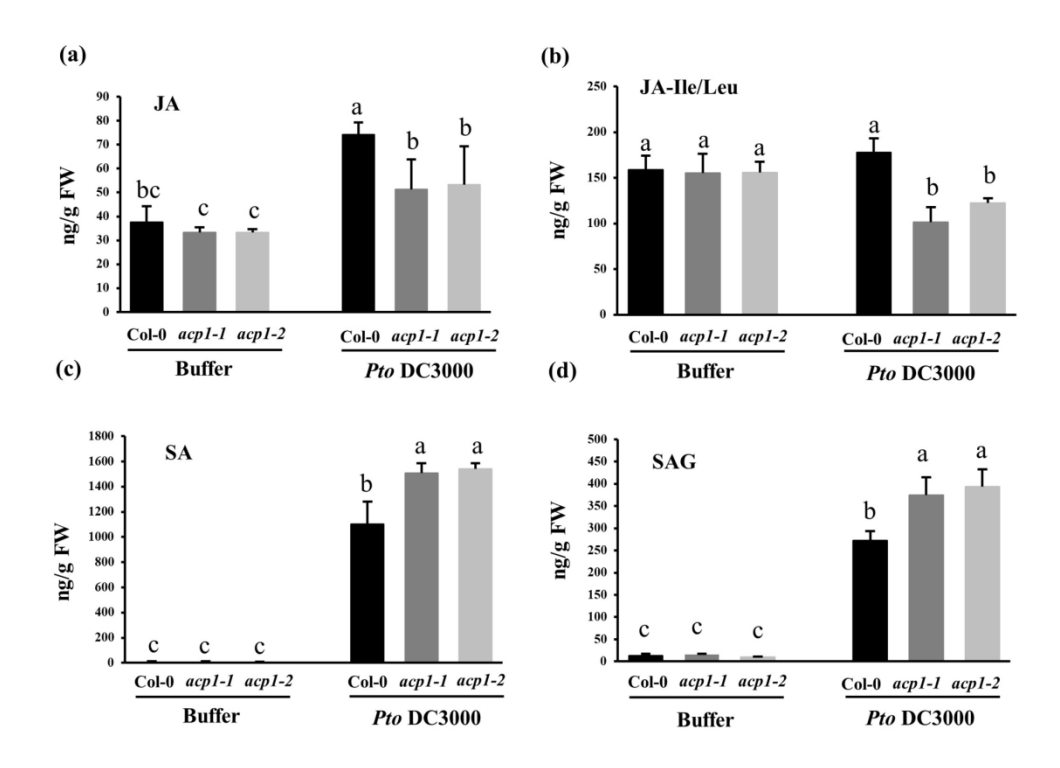


Figure 5. The acp1 mutants accumulated a higher level of salicylic acid (SA) and a lower level of jasmonic acid (JA) after the pathogen Pto DC3000 infection. WT and acp1 mutant plants were inoculated with the buffer (10 mM MgCl<sub>2</sub>) or Pto DC3000 at  $5\times10^5$  CFU/ml by leaf infiltration. Leaf samples were collected for quantification of free JA (a) and JA-Ile/Leu (JA-isoleucine/leucine) (b), free SA (c), and SAG (SA-glycoside) (d) at 48 hours post-inoculation. Data represent means  $\pm$  SE (n = 4), which are from one of the three independent repeats with consistent results. Different letters a-c within the figure (a-d) indicate the significant differences at p < 0.05, which was calculated by one-way analysis of variance (ANOVA) using SPSS ver. 21.

164x135mm (300 x 300 DPI)

Figure 6.

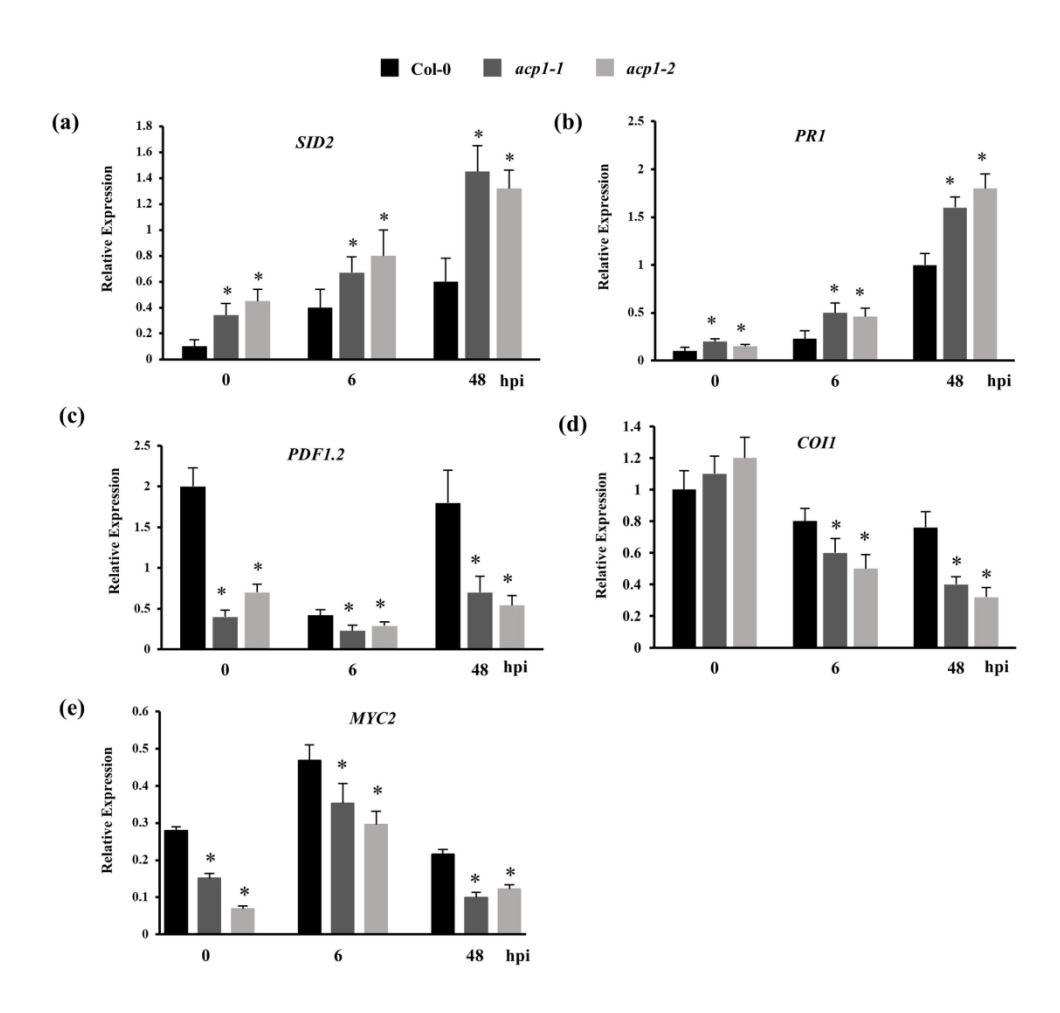
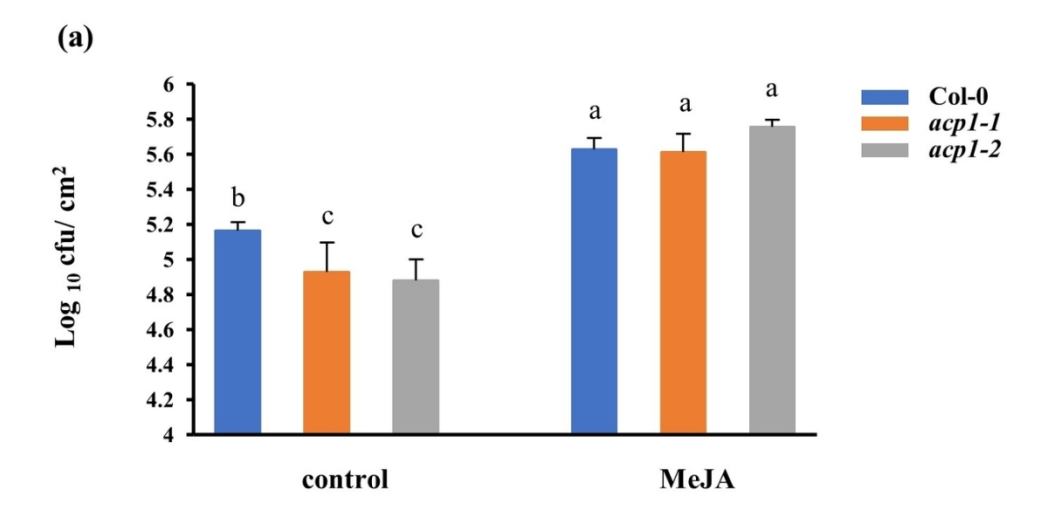


Figure 6. The acp1 mutants showed the enhanced SA-related gene expression and reduced JA-related gene expression after the Pto DC3000 treatment. After the inoculation with Pto DC3000 at  $5\times10^5$  CFU/ml by infiltration, the total RNA was extracted from the inoculated leaves of WT Col-0 and acp1 mutants at the indicated times. The relative transcriptional levels of SID2 (a), PR1 (b), PDF1.2 (c), COI1 (d), and MYC2 (e) were determined by qPCR with UBIQUITIN as the internal reference gene. Data represent means  $\pm$  SE (n = 4), which are from one of the three independent repeats with consistent results. Significant differences between the WT and acp1 mutants were indicated by the asterisks determined from the Student's t-test (p < 0.05).

163x175mm (300 x 300 DPI)

### Figure 7.



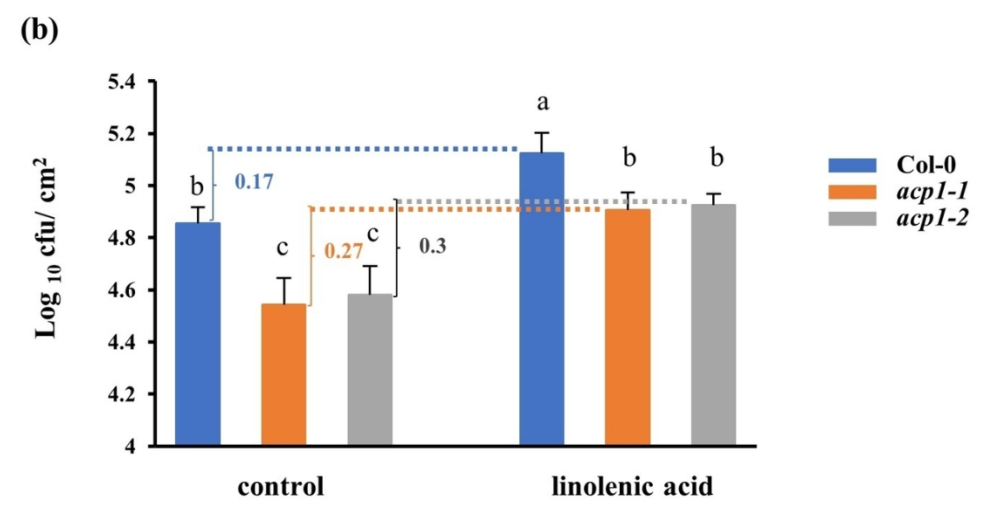


Figure 7. Effects of MeJA and C18:3 FA (linolenic acid) treatments on the plant defense of acp1 mutants against Pto DC3000. Four-week-old WT Col-0 and acp1 plants were sprayed with solvent control (0.1% ethanol) or 50  $\mu$ M MeJA or 0.1 mM linolenic acid. Plants were syringe infiltrated with  $5\times10^5$  CFU/mL of Pto DC3000 24 hours after treatments. The bacterial multiplication in the leaves of WT and acp1 mutants was checked three days after the inoculation (a &b). Data represent means  $\pm$  SE (n = 4), which are from one of three independent repeats with consistent results. Different letters a-c within the figures indicate the significant differences at p < 0.05, calculated by one-way analysis of variance (ANOVA) using SPSS ver. 21.

109x131mm (300 x 300 DPI)



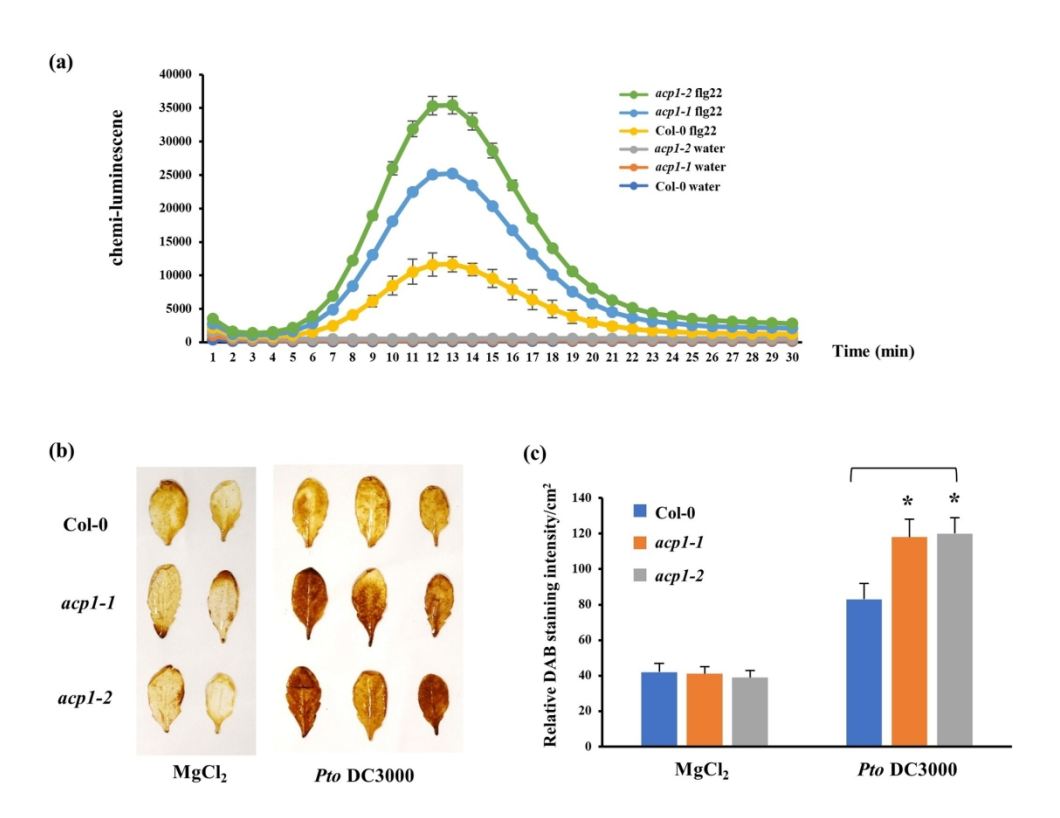
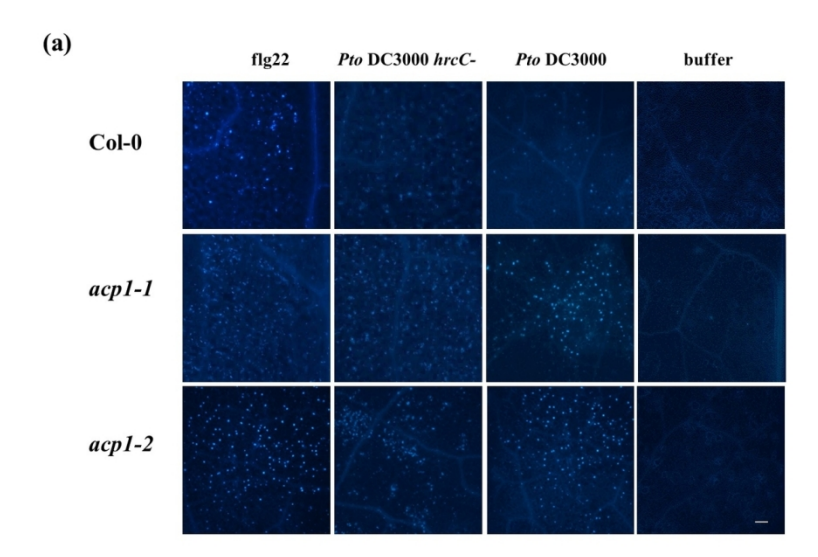


Figure 8. The acp1 mutants showed enhanced  $H_2O_2$  accumulation upon the MAMP flg22 treatment or Pto DC3000 inoculation (a). The real-time chemiluminescence of  $H_2O_2$  burst curve upon the 100 nM flg22 induction or water treatment. Leaf discs (5 mm in diameter) were pre-treated with water overnight. Pre-treated leaf discs were treated with 100 nM flg22 in the buffer, which contained the luminol and horseradish peroxidase or mock treatment (water). Luminescence was recorded for 30 mins using the GLOMAX luminometer. Data represent means  $\pm$  SE (n = 5), which are from one of the two independent repeats with consistent results. (b). WT Col-0 and acp1 mutant plants were sprayed with Pto DC3000 ( $10^7$  CFU/ml) or with buffer (10 mM MgCl<sub>2</sub>) as the control. The  $H_2O_2$  production was visualized by the 3,3-diaminobenzidine tetrahydrochloride (DAB) staining at 48 hours post-inoculation. The brown color indicated the  $H_2O_2$  production site. (c) The production of  $H_2O_2$  upon Pto DC3000 infection and buffer treatment is indicated by the DAB staining intensity. Data represent means  $\pm$  SE (n = 3), which are from one of the three independent repeats with consistent results. Significant differences between the WT and acp1 mutants were indicated by the asterisks determined from the Student's t-test (p < 0.05).

162x141mm (300 x 300 DPI)

Figure 9.



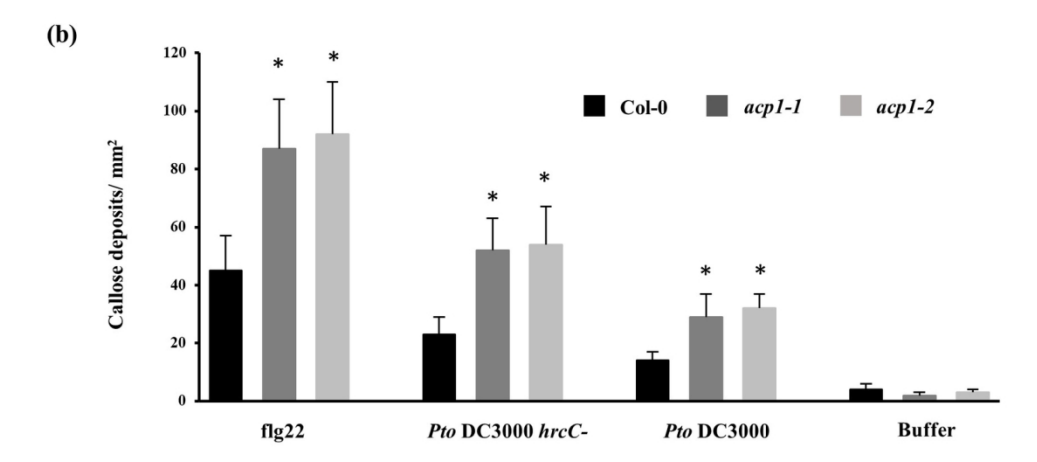


Figure 9. The acp1 mutants showed the enhanced callose deposition in response to the MAMP treatment and the pathogen Pto infection. The leaves of acp1 mutants and WT Col-0 plants were infiltrated with the buffer (10 mM MgCl<sub>2</sub>), 100  $\mu$ M flg22, Pto DC3000 at  $10^8$  CFU/ml, and Pto DC3000  $hrcC^-$  at  $10^8$  CFU/ml. Callose deposition quantification was determined by staining the leaves with 0.01% aniline blue solution 16 hours after inoculation. (a). The images of callose deposition in Arabidopsis leaves. (b). The number of callose deposition points was quantified by Image J software. The numbers shown are mean callose deposits per mm<sup>2</sup> from six images. Data represent means  $\pm$  SE (n = 12), which are from one of the three independent repeats with consistent results. Significant differences between the acp1 mutants and WT were indicated by the asterisks determined from the Student's t-test (p < 0.05).

137x158mm (300 x 300 DPI)

#### **1 Supporting Material**

- 2 Involvement of Arabidopsis Acyl Carrier Protein 1 in PAMP-triggered immunity
- 3 Zhenzhen Zhao<sup>1</sup>, Jiangbo Fan<sup>1,2</sup>, Piao Yang<sup>1</sup>, Zonghua Wang<sup>3</sup>, Stephen Obol Opiyo<sup>1</sup>, David
- 4 Mackey<sup>4</sup>, Ye Xia<sup>1,\*</sup>

- 6 <sup>1</sup>Department of Plant Pathology, The Ohio State University, 2021 Coffey Road, Columbus, OH
- 7 43210, U.S.A.
- 8 <sup>2</sup>School of Agriculture and Biology, Shanghai Jiao Tong University, 800 Dongchuan Rd.,
- 9 Shanghai, 200240, China
- <sup>3</sup>State Key Laboratory of Ecological Pest Control for Fujian and Taiwan Crops, Fujian Agriculture
- and Forestry University, Fuzhou, 350002, China
- <sup>4</sup>Department of Horticulture and Crop Science, The Ohio State University, Columbus, OH 43210,
- 13 U.S.A.
- \* Corresponding author: Ye Xia; Email: xia.374@osu.edu
- 15 **Keywords:** acyl carrier protein, fatty acids, plant immunity, PTI, plant hormones
- Author contributions: Conceptualization, Z.Z., D.M., and Y.X.; methodology, Z.Z., D.M., and
- 17 Y.X.; software, S.O.; formal analysis, Z.Z.; investigation, Z.Z., J.F., P.Y., Z.W., and X.Y.; data
- curation, Z.Z.; writing—original draft preparation, Z.Z.; writing—review and editing, Z.Z., D.M.,
- and Y.X.; visualization, Z.Z.; supervision, Z.Z., D.M., and Y.X.; project administration, Z.Z. and
- 20 Y.X.; and funding acquisition, D.M. and Y.X. All authors have read and agreed to the published
- 21 version of the manuscript.



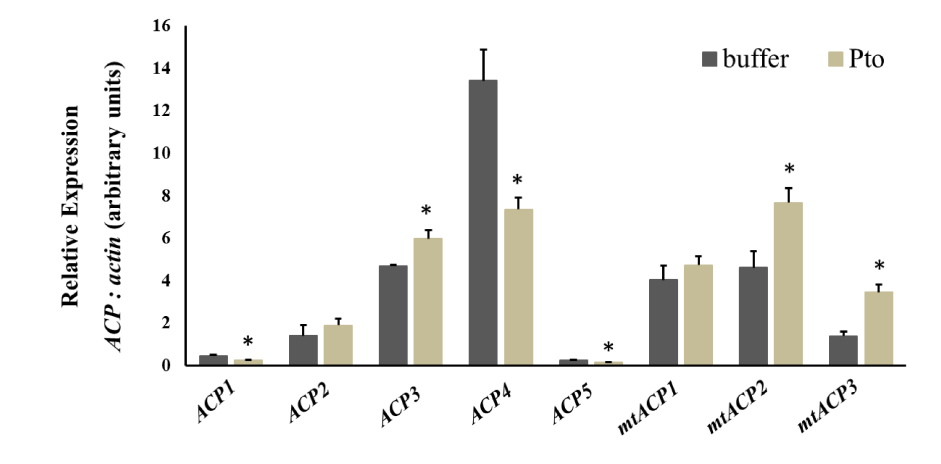


**Figure S1.** The relative transcriptional levels of ACPs in response to the bacterial pathogen Pto DC3000 infection. Col-0 leaves were infiltrated with buffer and  $5\times10^5$  CFU/mL of Pto DC3000. Quantitative real-time PCR (qPCR) was used to measure the amount of ACPs transcript (relative to ACTIN) at 6 hours post-inoculation. Data represent means  $\pm$  SE (n = 4), which are from one of the three independent repeats with consistent results. Significant differences between the WT and acp1 mutants were indicated by the asterisks determined from the Student's t-test (p < 0.05).

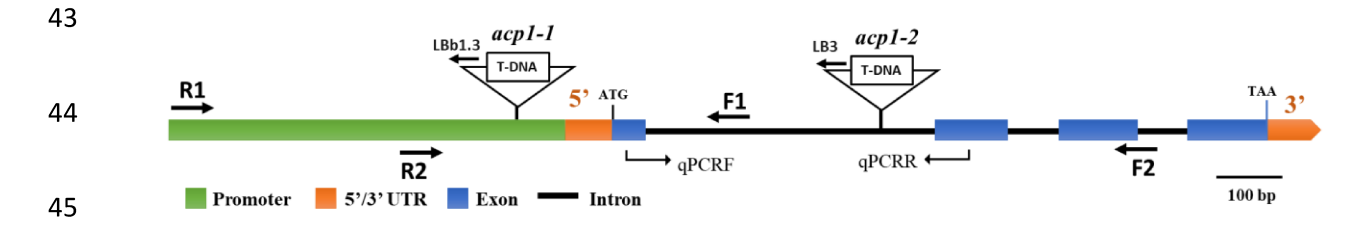


Figure S2. The diagram of the *ACP1* genomic structure and T-DNA insertion sites in two *acp1* mutants. The position and orientation of primers used for PCR confirmation of the *acp1-1* (F1 and R1) and *acp1-2* mutants (F2 and R2) are marked by arrows. LBa1.3 and LB3 (left border primer) are specific for the T-DNA sequence of *acp1-1* and *acp1-2* mutants, respectively. The position and orientation of primers used for qRT-PCR are indicated as qPCRF and qPCRR.

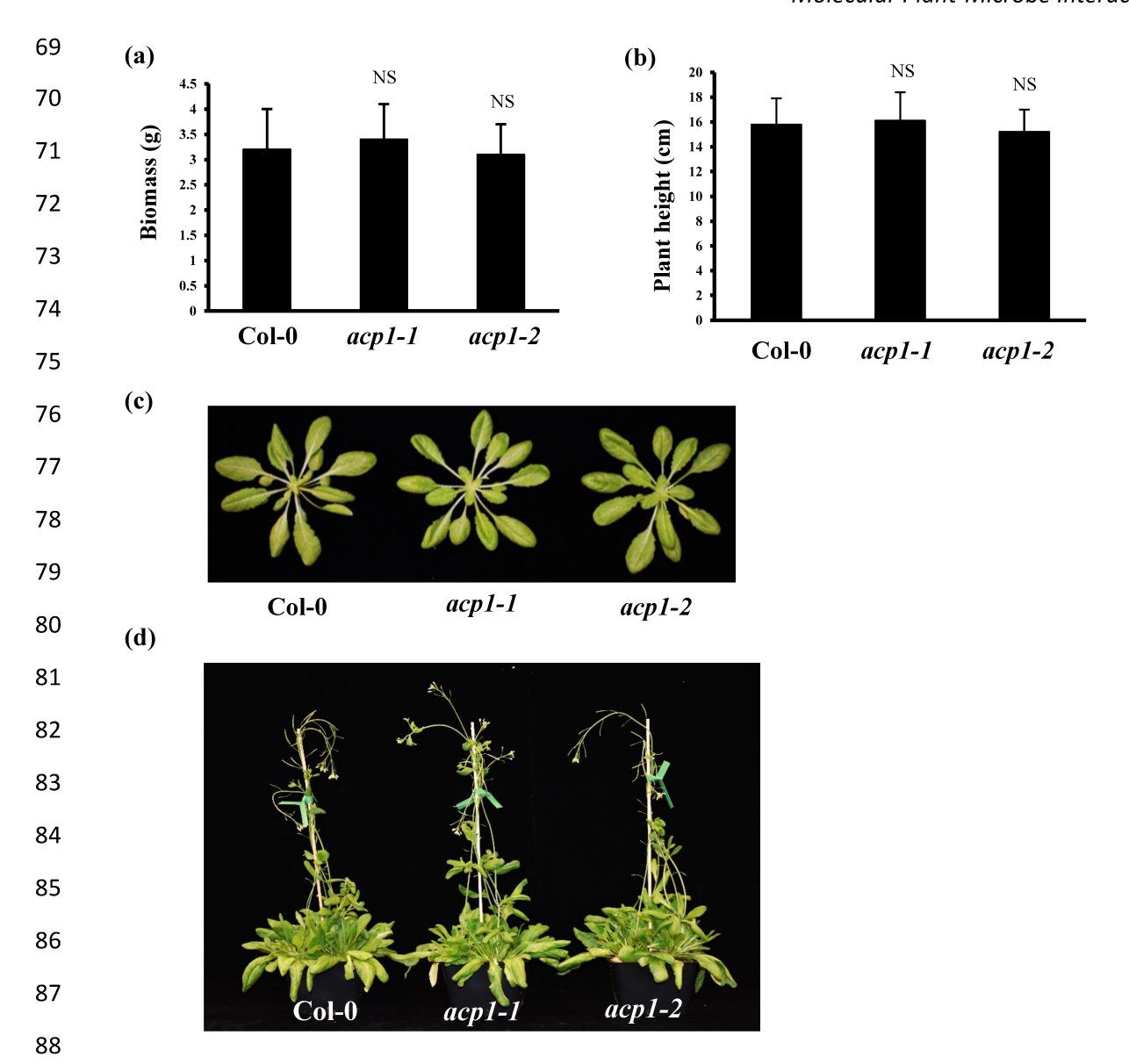


Figure S3. The physiological parameters of the acp1 mutants and WT plants. (a). Plant biomass (weight) of the acp1 mutants and WT plants. (b). Plant height of the acp1 mutants and WT plants. Data represent means  $\pm$  SE (n = 4), which are from one of the two independent repeats with consistent results. Significant differences between the acp1 mutants and WT were indicated by the asterisks determined from the Student's t-test (p < 0.05). NS represents no significance. (c). Morphological phenotypes of rosettes from 4-week-old acp1 mutants and WT plants. (d). Morphological phenotypes of the 6-week-old acp1 mutants and WT plants.

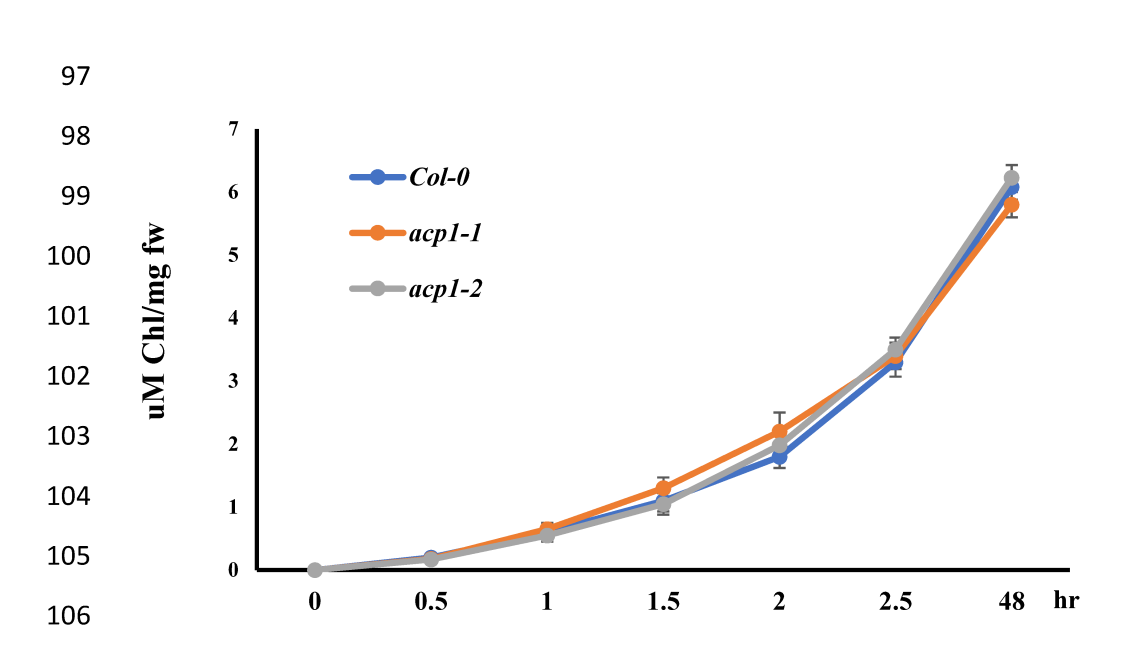


Figure S4. Chlorophyll content and chlorophyll leaching rate of WT plant leaves (blue circles), acp1-1 mutant (orange circles), and acp1-2 mutant (grey circles). The acp1 mutants showed similar chlorophyll content and chlorophyll leaching rate to the WT Col-0. Data represent means  $\pm$  SE (n = 3), which are from one of the three independent repeats with consistent results. Significant differences between the acp1 mutants and WT were indicated by the asterisks determined from the Student's t-test (p < 0.05).

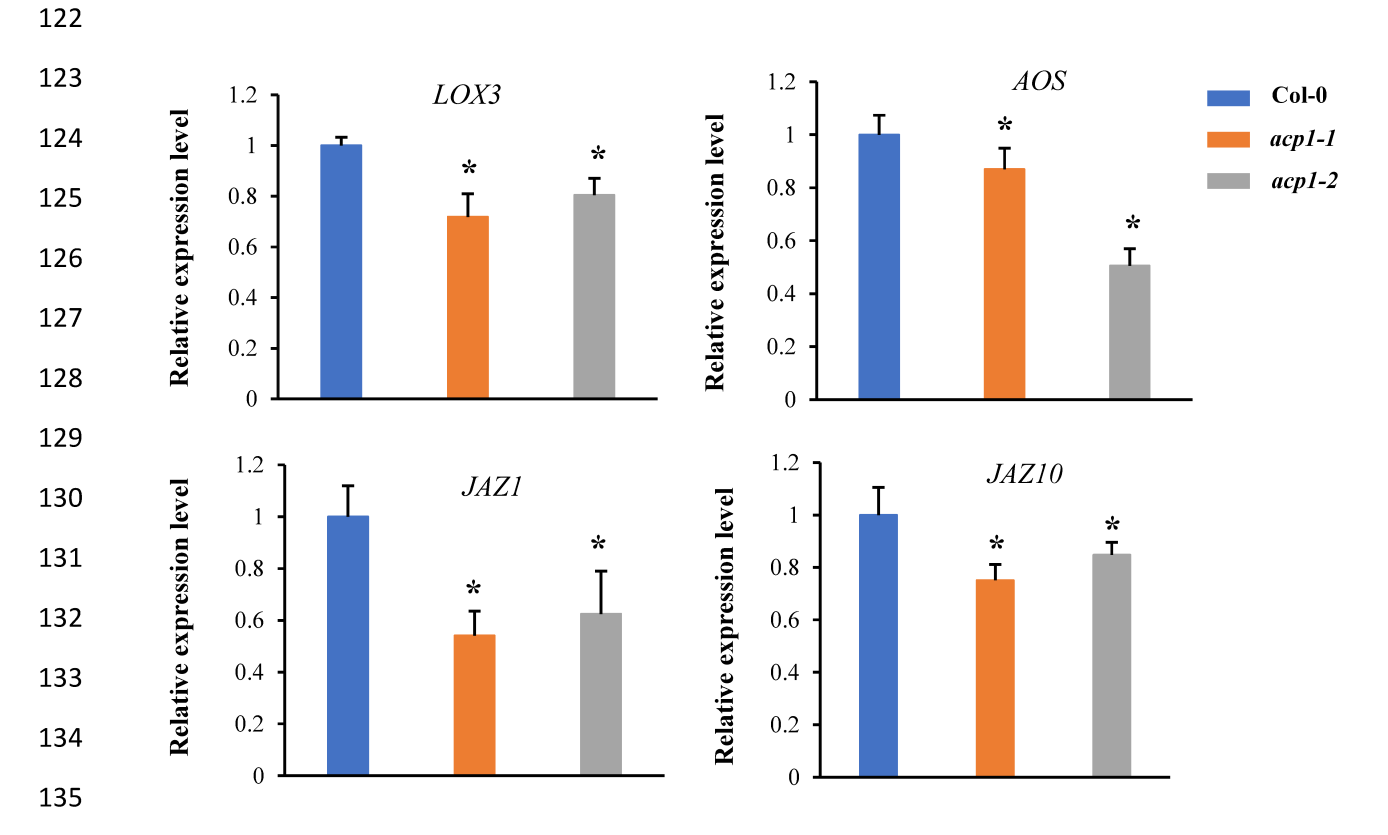


Figure S5. Basal transcript levels of JA-related genes in 4-week-old *acp1* mutants and WT plant leaves. The JA biosynthesis genes LOX3, AOS, and JA downstream signaling genes JAZ1 and JAZ10 were quantified by qRT-PCR and normalized to the expression of *ubiquitin*. Data represent means  $\pm$  SE (n = 4), which are from one of the three independent repeats with consistent results. Significant differences between the WT and acp1 mutants were indicated by the asterisks determined from the Student's t-test (p < 0.05).

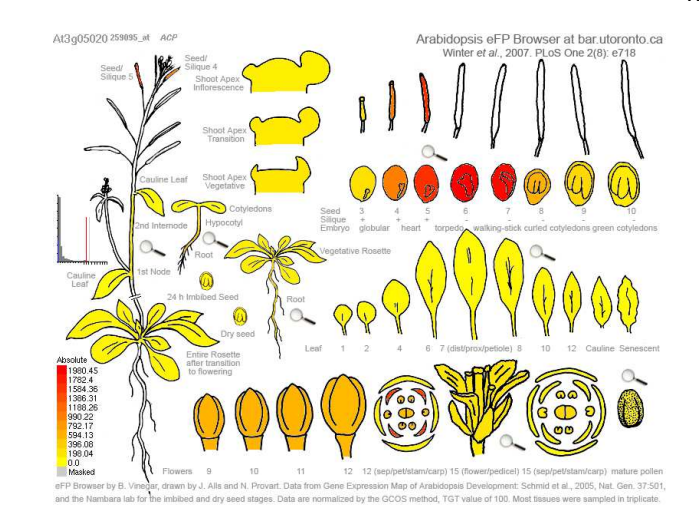


Figure S6. The *ACP1* gene expressions in different tissues of Arabidopsis plants. The *ACP1* gene expression at different tissues of the Arabidopsis plant is shown in different colors. Related information is obtained from Arabidopsis eFP Browser. http://bar.utoronto.ca/eplant/.

# 176 Table S1. The accession number list of ACP1 homologs

Species Name	Protein Sequence Accession Number in NCBI
Arabidopsis thaliana	NP_187153.1
Arabidopsis lyrata subsp. Lyrate	XP 020886365.1
Capsella rubella	XP_006299536.2
Camelina sativa	XP_010464003.1
Arabis nemorensis	VVA96518.1
Eutrema salsugineum	XP_006408119.1
Brassica oleracea var. oleracea	XP_013586447.1
Brassica rapa	XP_009124065.1
Arabis alpine	KFK37908.1
Raphanus sativus	XP_018438995.1
Brassica rapa subsp. Chinensis	ANS54496.1
Brassica cretica	RQL89968.1
Brassica oleracea var. oleracea	XP_013584173.1
Tarenaya hassleriana	XP_010524895.1
Eutrema salsugineum	XP_006394987.1
Populus euphratica	XP_011023489.1
Theobroma cacao	XP_007030153.1
Parasponia andersonii	PON73966.1
Populus trichocarpa	ABK93956.1
Durio zibethinus	XP_022718945.1
Populus alba	TKS10858.1

# 192 Table S2. The primer list for the PCR and RT-qPCR

Name	Sequence 5' to 3'	Purpose	
acp1-1-LP (F1)	TTTTAATTCCATGTGTTGCCG	acp1-1 T-DNA line genotyping	
acp1-1-RP (R1)	AGTTTGATGATGCCTTCATGC		
acp1-2-LP (F2)	ACGATAACAAGAGCAGGCATG	acp1-2 T-DNA line genotyping	
acp1-2-RP (R2)	CTCCGACTGAGAGAAGCAGCC	mp = = = = m = m = g = = y p = g	
LB3	TAGCATCTGAATTTCATAACCAATCTCGATACAC	T-DNA left border primer	
LBb1.3	ATTTTGCCGATTTCGGAAC	T-DNA left border primer	
ACP1GFP-F	CACGCTCGAGGAATTCATGATGGGTTGTTCGGTCTCGA AGATGACTCAATCTATCTGTTCGTC	Clone full-length CDS of ACP1 for	
ACP1GFP-R	GCTCACCATGGTGTTTGGTC	subcellular localization	
ACP1-qF	GCGGAGGTTGAAGGATAGATTA	qRT-PCR for ACP1 expression	
ACP1-qR	GCTTCTGTCTCATTGCAAACTT	pattern	
ACP2-qF	GGCC TTCTTTTAATCTCCGCGCCG	qRT-PCR for ACP2 expression pattern	
ACP2-qR	GCCGGCACCAAGTGCAGCAAGCTG	1	
ACP3-qF	GCGCTTCTTTTAATCTTCGCGCCG	qRT-PCR for ACP3 expression pattern	
ACP3-qR	CCGCGGGAATCAGCACCAAGGCCG	1	
ACP4-qF	ACAATGGAGATAGTGATGGCGTTG	qRT-PCR for ACP4 expression pattern	
ACP4-qR	CGGCAAACGCTCTGAAGGCAAGAA	- Panton	
ACP5-qF	CCGCGGCTACGATTTTCAACGCGC	qRT-PCR for ACP5 expression pattern	
ACP5-qR	CCGCTCGGTAAATTTAGTTCGGCC		
MTACP1-qF	GGCGTTTCTTCGCACGATGAGCCG	qRT-PCR for <i>MTACP1</i> expression pattern	
MTACP1-qR	GCTGCCAGCTTGAATTCCTCGGCG		
MTACP2-qF	CGGCCGAGGAAGTTAGAGGCCGGC	qRT-PCR for MTACP2 expression pattern	
MTACP2-qR	GGGCAACCCAAATTCCTCCTCGCG	, p	
MTACP3-qF	GGCGTTTCACATCAGAAGCACGGC	qRT-PCR for <i>MTACP3</i> expression pattern	
MTACP3-qR	CCGCGAGAACTCTTCTTCAAGCCG	pattern	
SID2-qF	CACGGAGTGTCCCACTTCG		
SID2-qR	CGTCATGTCATCAGCGGTATC	RT-qPCR test	

# Zhenzhen Zhao *Molecular Plant-Microbe Interactions*®

PR1-qF	GGCTCATATACCTCTGCACTCTA	
PR1-qR	TGGTTTAGATACTCTGCTACGGC	
PDF1.2-qF	AATAGGAATTGATCCAGTCGCAG	RT-qPCR test
PDF1.2-qR	CTTTCGTCGCCTTACACTCTTT	K1-qrCK test
ACTIN-qF	ATCCAATCCTCCCCAACACC	
ACTIN-qR	AACTCTGTCCTTTCTCCC	
UBIQUITIN-qF	AGATCCAGGACAAGGAGGTATTC	
UBIQUITIN-qR	CGCAGGACCAAGTGAAGAGTAG	